

分肝移植術（ABO 血液型不適合）の予定となった。

術前準備：ドナー血液型 B 型，レシピエント血液型 O 型。生体肝移植手術施行 2 週間前に rituximab (300 mg/body) で投与し，その翌日から tacrolimus 0.8 mg 分 2，mycophenolate mofetil (MMF) を 750 mg 分 2 で移植前日まで内服した。手術施行 2 日前より血液浄化を行った。2 回の血液浄化後，血型抗体価は 64 倍から 1 倍未満となり予定通り生体肝移植術を施行した。
手術所見（1 回目）：レシピエント肝を全摘出し，母の肝左葉をグラフトとして移植した。グラフト重量 234 g，グラフト・レシピエント体重比 (graft-to-recipient body weight ratio: GRWR) は 0.9%。脾臓摘出は行わず，上腸間膜静脈の一部より門脈カテーテルを挿入して術中門脈血圧を測定したところ 25-30 mmHg と高かったため，それ以上の門脈血流は必要ないと判断し，術前より確認されていた左胃静脈のシャント処理は行わなかった。術後治療のために，門脈カテーテルを留置したまま手術終了とした。

術後経過：術後からドップラー超音波による血流評価を行い，肝動脈・門脈・肝静脈のいずれも血流は良好であった。門脈カテーテルより tacrolimus，methylprednisolone を持続投与した。

手術所見（2 回目）：術後 7 日目，全身麻酔下に門脈カテーテル抜去と肝左側に留置してあった腹腔ドレーン抜去を行った。

術後経過（2 回目）：術後のドップラー超音波による評価では血流を認めたが，翌日に行ったドップラー超音波で門脈血流を認めず（図 1a），門脈血栓を疑い造影 CT 検査を施行したところ，門脈血栓は認めず造影剤による門脈濃染像を認めた（図 1b）。

血行動態の把握のために perflubutane（ソナゾイド®）0.3 ml を投与し造影超音波を施行したところ，門脈内に造影剤の血流を認めた（図 1c）。術前より認められた左胃静脈からの門脈体循環シャントによる門脈盗血を起こしたと考え，免疫抑制剤の増量，輸液負荷・輸血によりドップラー超音波でも若干の血流改善を認めた。しかしながら，輸液負荷や輸血を行わないとドップラー超音波ではすぐに血流が確認できなくなり，輸血量が多くなるとや長期に免疫抑制剤の量を上げることによる易感染状態を促すことにより術後の感染症が致命傷となることを懸念し血行郭清を行うこととした。

手術所見（3 回目）：前回手術創から開腹した。癒着を剥離しながら門脈を確認して門脈を末梢側へと追っていき，怒脹した左胃静脈を確認した。左胃静脈を二重結紮し，門脈血流の改善を確認した（図 2a, b, c）。肝生検を行い，閉腹した。

病理所見（図 3）：術中肝生検の結果で門脈の拡大を認め，周囲にリンパ球の増生を認めた。胆管の周囲にはリンパ球浸潤は認めるも胆管上皮の変化はあまり目

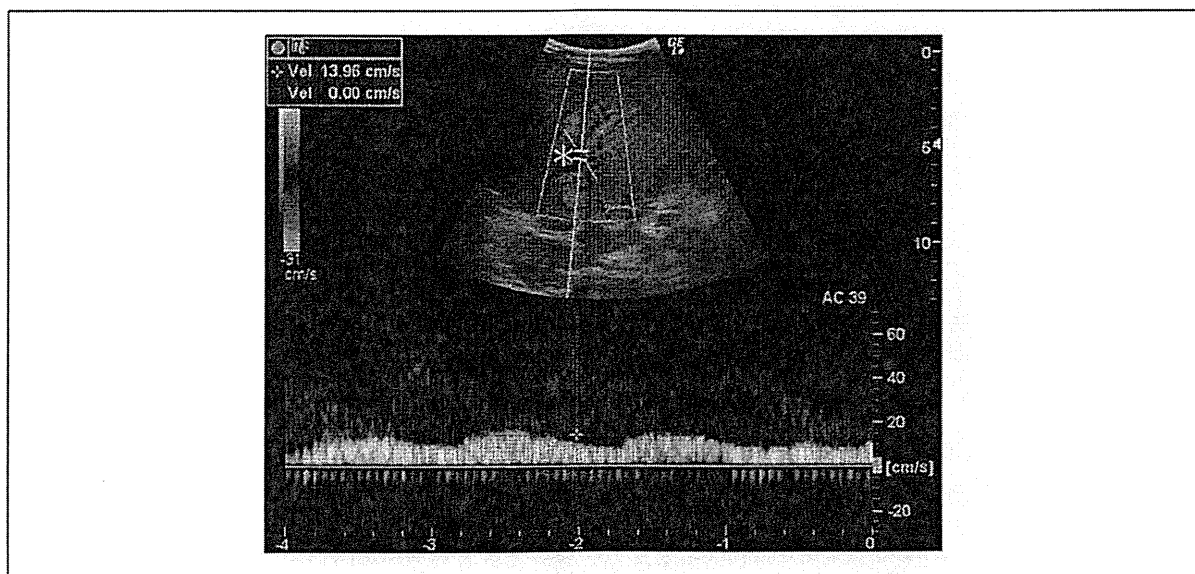


図 1a 2 回目手術翌日の門脈血流を認めないドップラー超音波
肝動脈（赤色）の血流のみが目立ち，門脈（*）は黒く抜けている。

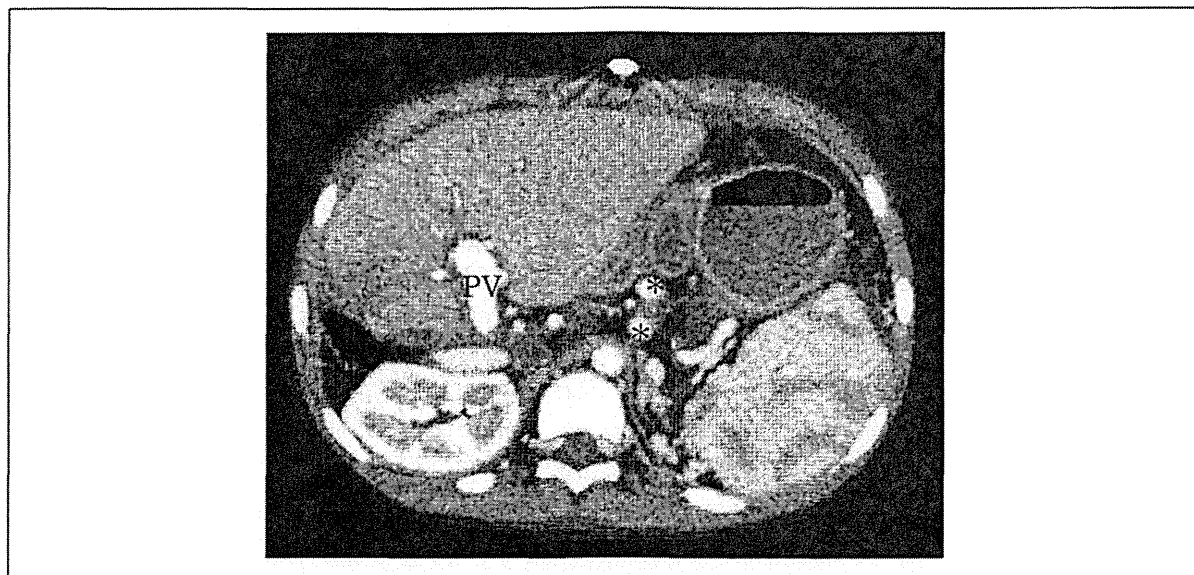


図 1b 同時期の造影 CT の所見：門脈濃染像

門脈 (PV) は造影剤により濃染されており、門脈内に血栓は認めない。左胃静脈 (*) が怒張して残っている (蛇行して 1 スライスに 2 箇所認めている)。

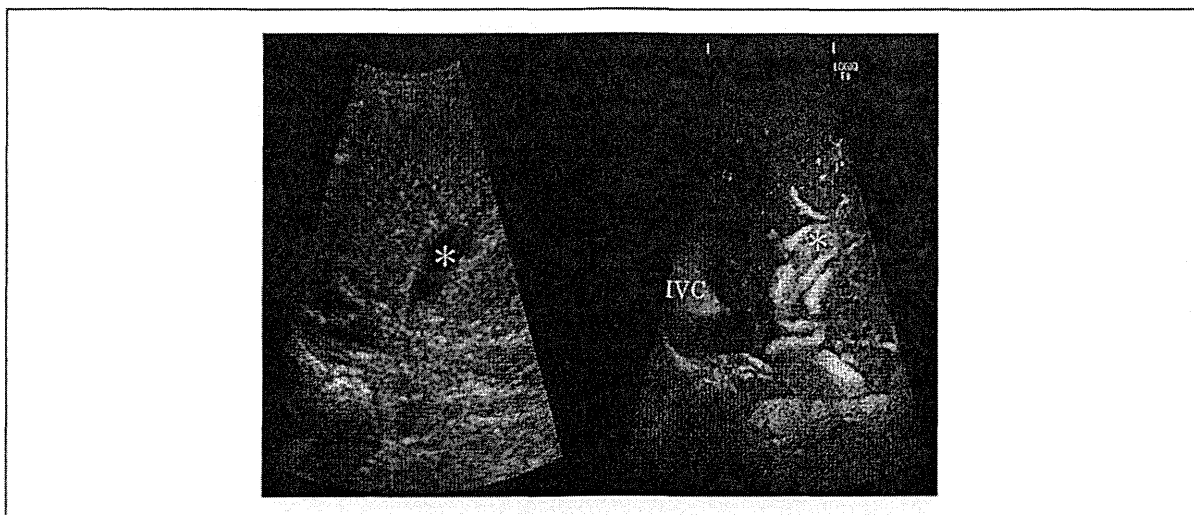


図 1c 造影超音波による門脈濃染像

左が通常の B モード。右が造影超音波。造影剤を投与してすぐに門脈 (*) 周囲にまわりつくようにある動脈に造影剤が流入し、次いで門脈に順行性に造影剤が流れ込むのを確認した。IVC：下大静脈

立たなかったが、中心静脈周囲のリンパ球浸潤を認め、急性拒絶の所見であった (Banff schema 分類 Rejection Activity Index 5 点)。肝実質内に出血やフィブリンの沈着は認めず抗体関連型拒絶の所見は認めなかった。

術後経過 (3 回目)：ステロイドパルス (10 mg/kg ポー

ラス投与×3 日間) を施行した。また肺内シャントの増悪もあり、輸液管理とレートコントロールを厳密に行うことで、門脈血流と肺内シャントの改善を認め、術後 3 カ月で門脈の吻合部狭窄は認めるが (図 4)、他問題なく経過している。

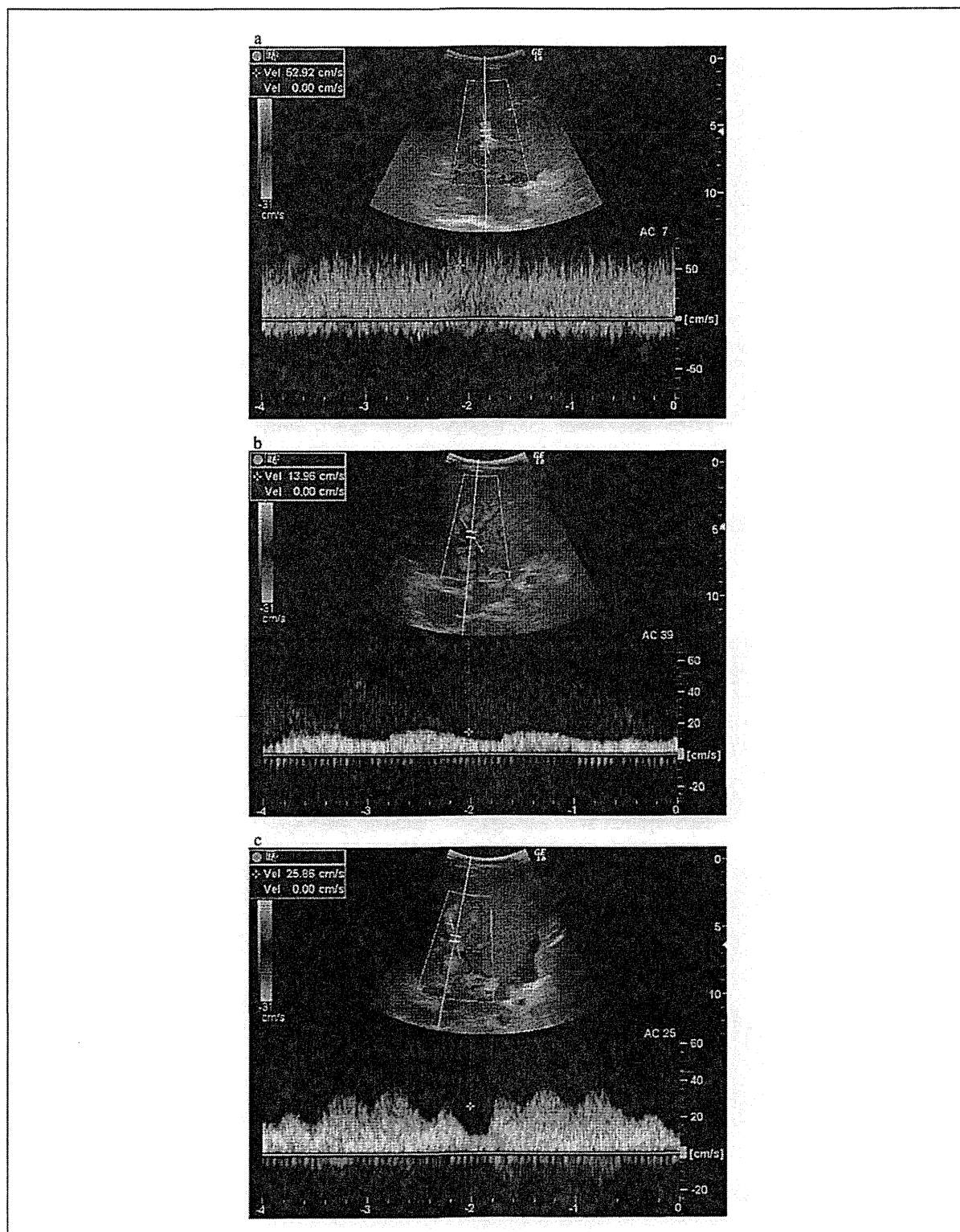


図2 ドップラー超音波の経過

- a: 1回目の手術後。門脈は定常流で流速も十分認める。
 b: 2回目の手術翌日。門脈のカラーが抜けており、流速は10 cm/sec程度で周囲の動脈波形も拾っている。
 c: 3回目の手術後。門脈は呼吸性変動を強く受け、鋸歯状波で拒絶を示唆する。

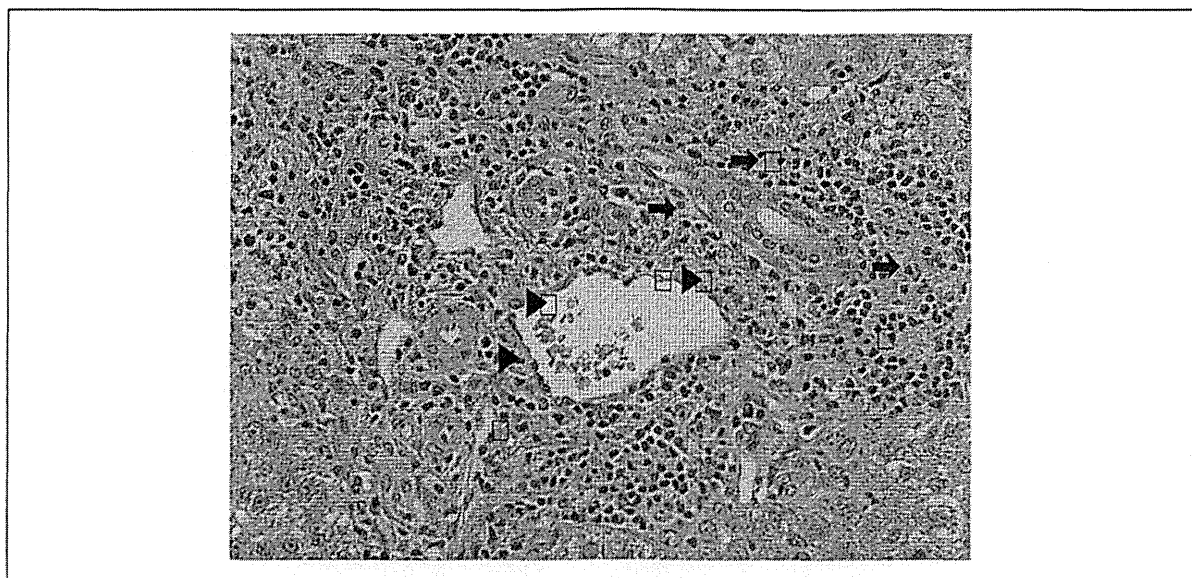


図3 肝生検病理

門脈流域(▶□)にCD3陽性リンパ球の浸潤を認めた。胆管(⇒□)周囲にもリンパ球を認めたが、胆管上皮の変化はあまり認めなかった。

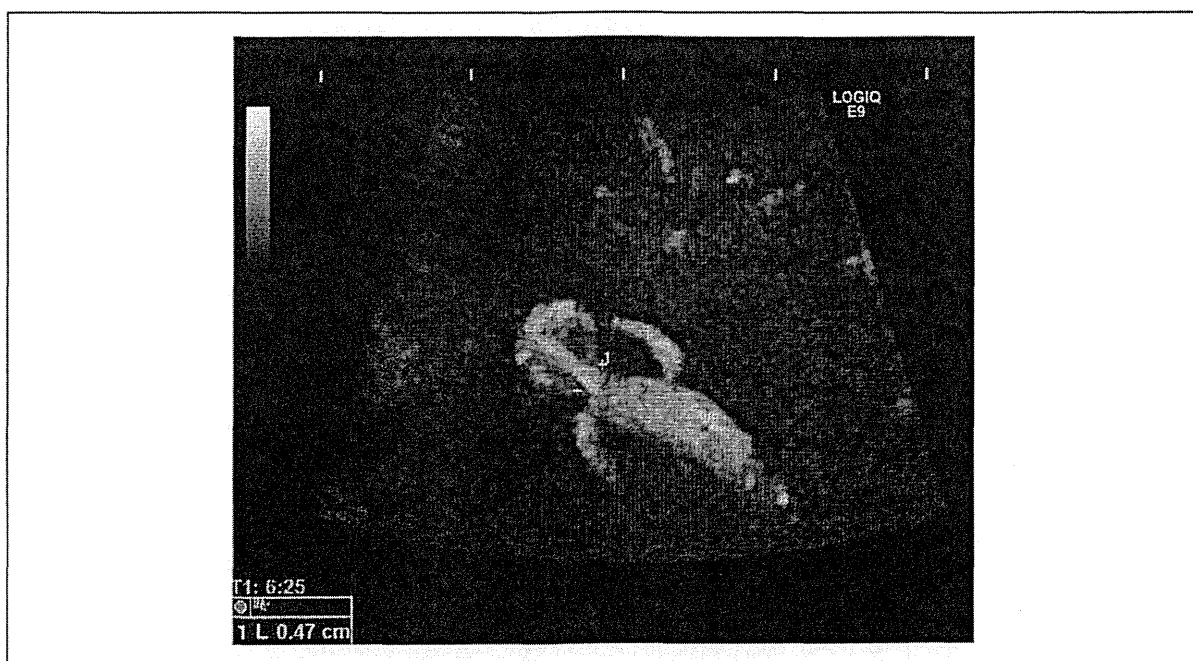


図4 退院前の造影超音波像

門脈内に造影剤が流入している。門脈の吻合部に狭窄(十一十、径4.7mm)を認める。

Ⅲ. 考 察

小児生体肝移植術後の門脈合併症は約10%に生じ

るとされる^{1,2)}。門脈体循環シャントには冠静脈シャント、脾腎シャント、臍静脈シャントの3種類がある。門脈盗血は門脈体循環シャントの遺残と急性拒絶や重

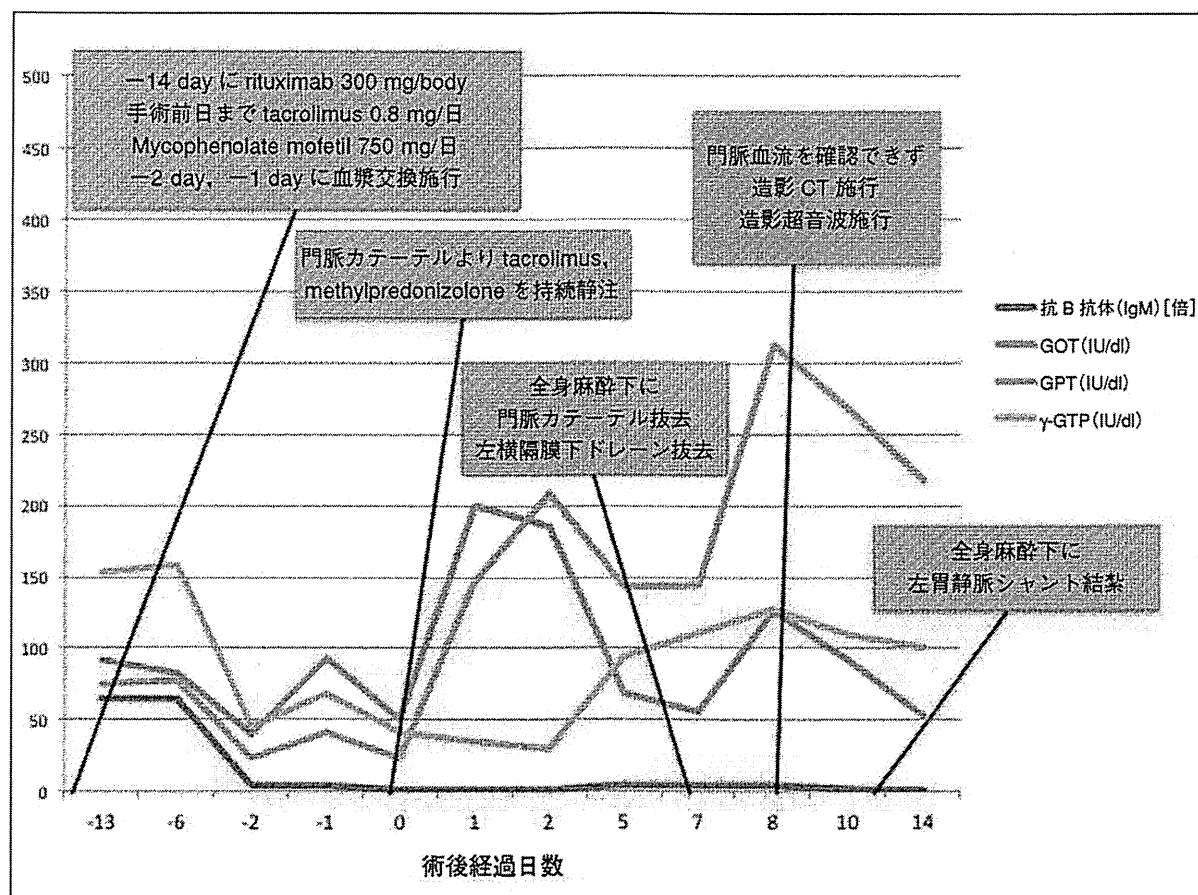


図5 生体肝移植施行日を0日とした術後経過

術後7日目に全身麻酔下に門脈カテーテルおよび左横隔膜ドレーンを抜去し、翌日に超音波ドップラーで門脈血流を認めなくなった。門脈盗血と判断し、輸液負荷・輸血および免疫抑制剤の増量を行うも、顕著な改善なく、術後11日目に全身麻酔下に左胃静脈シャントを結紮した。

度の虚血性障害による門脈高血圧が原因であり、脾臓シャントを除いて手術中に結紮してくることが奨められている⁹⁾が、過小グラフトに対する高い門脈血流の弊害も指摘されており、門脈血流のコントロールにはいまだ課題が残っている¹⁰⁾。

自験例においても、門脈カテーテル抜去後に肝への免疫抑制剤の濃度が減少したことで、急性拒絶が増悪し門脈圧の上昇により初回手術時に処理をしなかった左胃静脈へのシャントが増えたと考えられる。

本邦で1999年に発売された静注用超音波造影剤レボリスト®(バイエル社)により肝臓領域を中心とした造影超音波検査が確立され、第二世代超音波造影剤としてソナゾイド®(第一三共社)が発売された。ソナゾイド®はperflubutaneと水素添加卵黄ホスファチジルセリンナトリウムから成るマイクロバブルであ

り、卵アレルギー患者以外では特に禁忌はなく、ベッドサイドで行えて放射線被曝やヨードへの曝露がない検査である。近年、肝臓移植においても造影超音波の有用性についての報告が増えてきている^{3,7,12)}。

ドップラー超音波による術後移植肝の血流評価は確立されており、成人肝移植における肝動脈塞栓の検出感度は92-96%とされているが、小児では対象も小さく描出が困難な場合も多い。従来のドップラー超音波で認められない場合に造影超音波を行うことで、肝動脈塞栓をより正確に診断できるとの報告もある^{3,4)}。門脈においてもより正確な血管径や吻合部狭窄の程度を見ることができる⁵⁾。本邦における肝移植後の血流評価に対して造影超音波を利用した報告はなく、今後の普及が期待される。

IV. 結 語

ドップラー超音波や造影CTだけでは病態の理解が不十分な場合もある。造影超音波検査は放射線被曝もなく、患者移送も必要のない検査であり、生体肝移植術後における血流評価として造影超音波による検索は診断に非常に有用であった。

なお、本論分の要旨は第50回日本移植学会総会にて発表した。

文 献

- 1) Ueda M, Oike F, Kasahara M, *et al.* Portal vein complications in pediatric living donor liver transplantation using left-side grafts. *Am J Transplant* 2008; 8: 2097-2105.
- 2) Moon JI, Jung GO, Choi GS, *et al.* Risk factors for portal vein complications after pediatric living donor liver transplantation with left-sided grafts. *Transplant Proc* 2010; 42: 871-875.
- 3) Hom BK, Shrestha R, Palmer SL, *et al.* Prospective evaluation of vascular complications after liver transplantation: comparison of conventional and microbubble contrast-enhanced US. *Radiology* 2006; 241: 267-274.
- 4) Bonini G, Pezzotta G, Morzenti C, *et al.* Contrast-enhanced ultrasound with SonoVue in the evaluation of postoperative complications in pediatric liver transplant recipients. *J Ultrasound* 2007; 10: 99-106.
- 5) Luo Y, Fan YT, Lu Q, *et al.* CEUS: a new imaging approach for postoperative vascular complications after right-lobe LDLT. *World J Gastroenterol* 2009; 15: 3670-3675.
- 6) Zheng RQ, Mao R, Ren J, *et al.* Contrast-enhanced ultrasound for the evaluation of hepatic artery stenosis after liver transplantation: potential role in changing the clinical algorithm. *Liver Transpl* 2010; 16: 729-735.
- 7) Rennert J, Dornia C, Georgieva M, *et al.* Identification of early complications following liver transplantation using contrast enhanced ultrasound (CEUS). First results. *J Gastrointest Liver Dis* 2012; 21: 407-412.
- 8) Sadamori H, Yagi T, Matsukawa H, *et al.* The outcome of living donor liver transplantation with prior spontaneous large portasystemic shunts. *Transpl Int* 2008; 21: 156-162.
- 9) Kiuchi T, Tanaka K, Ito T, *et al.* Small-for-size graft in living donor liver transplantation: how far should we go? *Liver Transpl* 2003; 9: S29-S35.
- 10) Lo CM, Liu CL, Fan ST. Portal hyperperfusion injury as the cause of primary nonfunction in a small-for-size liver graft-successful treatment with splenic artery ligation. *Liver Transpl* 2003; 9: 626-628.
- 11) 秋丸琥甫. 生体肝移植の問題点—特に過小グラフト対策について—. *日本医科大学医学会雑誌* 2005; 1: 156-160.
- 12) Ren J, Lu MD, Zheng RQ, *et al.* Evaluation of the microcirculatory disturbance of biliary ischemia after liver transplantation with contrast-enhanced ultrasound: preliminary experience. *Liver Transpl* 2009; 15: 1703-1708.

Prediction of interindividual differences in hepatic functions and drug sensitivity by using human iPS-derived hepatocytes

Kazuo Takayama^{a,b,c}, Yuta Morisaki^a, Shuichi Kuno^a, Yasuhito Nagamoto^{a,c}, Kazuo Harada^d, Norihisa Furukawa^a, Manami Ohtaka^e, Ken Nishimura^f, Kazuo Imagawa^{a,c,g}, Fuminori Sakurai^{a,h}, Masashi Tachibana^a, Ryo Sumazaki^g, Emiko Noguchiⁱ, Mahito Nakanishi^e, Kazumasa Hirata^d, Kenji Kawabata^{j,k}, and Hiroyuki Mizuguchi^{a,b,c,l,1}

^aLaboratory of Biochemistry and Molecular Biology; ^biPS Cell-based Research Project on Hepatic Toxicity and Metabolism; ^cLaboratory of Applied Environmental Biology; ^dLaboratory of Regulatory Sciences for Oligonucleotide Therapeutics, Clinical Drug Development Project, and ^eLaboratory of Biomedical Innovation, Graduate School of Pharmaceutical Sciences, Osaka University, Osaka 565-0871, Japan; ^fLaboratory of Hepatocyte Regulation, and ^gLaboratory of Stem Cell Regulation, National Institute of Biomedical Innovation, Osaka 567-0085, Japan; ^hResearch Center for Stem Cell Engineering, National Institute of Advanced Industrial Science and Technology, Ibaraki 305-8562, Japan; ⁱLaboratory of Gene Regulation, ^jDepartment of Child Health, and ^kDepartment of Medical Genetics, Faculty of Medicine, University of Tsukuba, Ibaraki 305-8575, Japan; and ^lThe Center for Advanced Medical Engineering and Informatics, Osaka University, Osaka 565-0871, Japan

Edited by Shinya Yamanaka, Kyoto University, Kyoto, Japan, and approved October 17, 2014 (received for review July 16, 2014)

Interindividual differences in hepatic metabolism, which are mainly due to genetic polymorphism in its gene, have a large influence on individual drug efficacy and adverse reaction. Hepatocyte-like cells (HLCs) differentiated from human induced pluripotent stem (iPS) cells have the potential to predict interindividual differences in drug metabolism capacity and drug response. However, it remains uncertain whether human iPS-derived HLCs can reproduce the interindividual difference in hepatic metabolism and drug response. We found that cytochrome P450 (CYP) metabolism capacity and drug responsiveness of the primary human hepatocytes (PHH)-iPS-HLCs were highly correlated with those of PHHs, suggesting that the PHH-iPS-HLCs retained donor-specific CYP metabolism capacity and drug responsiveness. We also demonstrated that the interindividual differences, which are due to the diversity of individual SNPs in the CYP gene, could also be reproduced in PHH-iPS-HLCs. We succeeded in establishing, to our knowledge, the first PHH-iPS-HLC panel that reflects the interindividual differences of hepatic drug-metabolizing capacity and drug responsiveness.

human iPS cells | hepatocyte | CYP2D6 | personalized drug therapy | SNP

Drug-induced liver injury (DILI) is a leading cause of the withdrawal of drugs from the market. Human induced pluripotent stem cell (iPSC)-derived hepatocyte-like cells (HLCs) are expected to be useful for the prediction of DILI in the early phase of drug development. Many groups, including our own, have reported that the human iPS-HLCs have the ability to metabolize drugs, and thus these cells could be used to detect the cytotoxicity of drugs that are known to cause DILI (1, 2). However, to accurately predict DILI, it will be necessary to establish a panel of human iPS-HLCs that better represents the genetic variation of the human population because there are large interindividual differences in the drug metabolism capacity and drug responsiveness of hepatocytes (3). However, it remains unclear whether the drug metabolism capacity and drug responsiveness of human iPS-HLCs could reflect those of donor parental primary human hepatocytes (PHHs). To address this issue, we generated the HLCs differentiated from human iPS cells which had been established from PHHs (PHH-iPS-HLCs). Then, we compared the drug metabolism capacity and drug responsiveness of PHH-iPS-HLCs with those of their parental PHHs, which are genetically identical to the PHH-iPS-HLCs.

Interindividual differences of cytochrome P450 (CYP) metabolism capacity are closely related to genetic polymorphisms, especially single nucleotide polymorphisms (SNPs), in CYP genes (4). Among the various CYPs expressed in the liver, CYP2D6 is responsible for the metabolism of approximately

a quarter of commercially used drugs and has the largest phenotypic variability, largely due to SNPs (5). It is known that certain alleles result in the poor metabolizer phenotype due to a decrease of CYP2D6 metabolism. Therefore, the appropriate dosage for drugs that are metabolized by CYP2D6, such as tamoxifen, varies widely among individuals (6). Indeed, in the 1980s, polymorphism in CYP2D6 appears to have contributed to the withdrawal of CYP2D6-metabolized drugs such as perhexiline from the market in many countries (7). If we could establish a panel of HLCs that better represents the diversity of genetic polymorphisms in the human population, it might be possible to determine the appropriate dosage of a drug for a particular individual. However, it is not known whether the drug metabolism capacity and drug responsiveness of HLCs reflect the genetic diversity, including SNPs, in CYP genes. Therefore, in this study we generated HLCs from several PHHs that have various SNPs on CYP2D6 and then compared the CYP2D6 metabolism capacity and responses to CYP2D6-metabolized drugs between the PHH-iPS-HLCs and parental PHHs.

Significance

We found that individual cytochrome P450 (CYP) metabolism capacity and drug sensitivity could be predicted by examining them in the primary human hepatocytes–human induced pluripotent stem cells–hepatocyte-like cells (PHH-iPS-HLCs). We also confirmed that interindividual differences of CYP metabolism capacity and drug responsiveness that are due to the diversity of individual single nucleotide polymorphisms in the CYP gene could also be reproduced in the PHH-iPS-HLCs. These findings suggest that interindividual differences in drug metabolism capacity and drug response could be predicted by using HLCs differentiated from human iPS cells. We believe that iPS-HLCs would be a powerful technology not only for accurate and efficient drug development, but also for personalized drug therapy.

Author contributions: K.T. and H.M. designed research; K.T., Y.M., and S.K. performed research; K.T., Y.M., Kazuo Harada, M.O., K.N., K.I., M.N., and Kazumasa Hirata contributed new reagents/analytic tools; K.T., Y.N., N.F., F.S., M.T., R.S., E.N., K.K., and H.M. analyzed data; and K.T. and H.M. wrote the paper.

The authors declare no conflict of interest.

This article is a PNAS Direct Submission.

Data deposition: The DNA microarray data reported in this paper have been deposited in the Gene Expression Omnibus (GEO) database, www.ncbi.nlm.nih.gov/geo (accession no. GSE61287).

¹To whom correspondence should be addressed. Email: mizuguch@phs.osaka-u.ac.jp.

This article contains supporting information online at www.pnas.org/lookup/suppl/doi:10.1073/pnas.1413481111/-DCSupplemental.

To this end, PHHs were reprogrammed into human iPSCs and then differentiated into the HLCs. To examine whether the HLCs could reproduce the characteristics of donor PHHs, we first compared the CYP metabolism capacity and response to a hepatotoxic drug between PHHs and genetically identical PHH-iPS-HLCs (12 donors were used in this study). Next, analyses of hepatic functions, including comparisons of the gene expression of liver-specific genes and CYPs, were performed to examine whether the hepatic characteristics of PHHs were reproduced in the HLCs. To the best of our knowledge, this is the first study to compare the functions between iPSC-derived cells from various donors and their parental cells with identical genetic backgrounds. Finally, we examined whether the PHH-iPS-HLCs exhibited a capacity for drug metabolism and drug responsiveness that reflect the genetic diversity such as SNPs on CYP genes.

Results

Reprogramming of PHHs to Human iPSCs. To examine whether the HLCs could reproduce interindividual differences in liver functions, we first tried to generate human iPSCs from the PHHs of 12 donors. PHHs were transduced with a Yamanaka 4 factor-expressing SeV (SeVdp-iPS) vector (*SI Appendix*, Fig. S1A) in the presence of SB431542, PD0325901, and a rock inhibitor, which could promote the somatic reprogramming (8). The reprogramming procedure is shown in *SI Appendix*, Fig. S1B. The human iPSCs generated from PHHs (PHH-iPSCs) were positive for alkaline phosphatase (*SI Appendix*, Fig. S1B, *Right*), NANOG, OCT4, SSEA4, SOX2, Tra1-81, and KLF4 (Fig. 1A). The gene expression levels of the pluripotent markers (*OCT3/4*, *SOX2*, and *NANOG*) in the PHH-iPSCs were approximately equal to those in human embryonic stem cells (ESCs) (*SI Appendix*, Fig. S1C, *Left*). The gene expression levels of the hepatic markers [*albumin (ALB)*, *CYP3A4*, and *α AT*] in the PHH-iPSCs were significantly lower than those in the parental PHHs (*SI Appendix*, Fig. S1C, *Right*). We also confirmed that the PHH-iPSCs have the ability to differentiate into the three embryonic germ layers in vitro by embryoid body formation and in vivo by teratoma formation (*SI Appendix*, Fig. S2A and B, respectively). To verify that the PHH-iPSCs originated from PHHs, short tandem repeat analysis was performed in the PHH-iPSCs and parental PHHs (*SI Appendix*, Fig. S2C). The results showed that the PHH-iPSCs were indeed originated from PHHs. Taken together, these results indicated that the generation of human iPSCs from PHHs was successfully performed. It is known that a transient epigenetic memory of the original cells is retained in early-passage iPSCs, but not in late-passage iPSCs (9). To examine whether the hepatic differentiation capacity of PHH-iPSCs depends on their passage number, PHH-iPSCs having various passage numbers were differentiated into the hepatic lineage (Fig. 1B). The *tyrosine aminotransferase (TAT)* expression levels and albumin (ALB) secretion levels in early passage PHH-iPS-HLCs (fewer than 10 passages) were higher than those of late passage PHH-iPS-HLCs (more than 14 passages). These results suggest that the hepatic differentiation tendency is maintained in early passage PHH-iPSCs, but not in late passage PHH-iPSCs. In addition, the hepatic functions of late passage PHH-iPS-HLCs were similar to those in the HLCs derived from late passage non-PHH-derived iPS cells (such as dermal cells, blood cells, and Human Umbilical Vein Endothelial Cells (HUVEC)-derived iPS cells) (*SI Appendix*, Fig. S3). Therefore, PHH-iPSCs, which were passaged more than 20 times, were used in our study to avoid any potential effect of transient epigenetic memory retained in parental PHHs on hepatic functions.

HLCs Were Differentiated from PHH-iPSCs Independent of Their Differentiation Tendency. To compare the hepatic characteristics among the PHH-iPS-HLCs that were generated from PHHs of

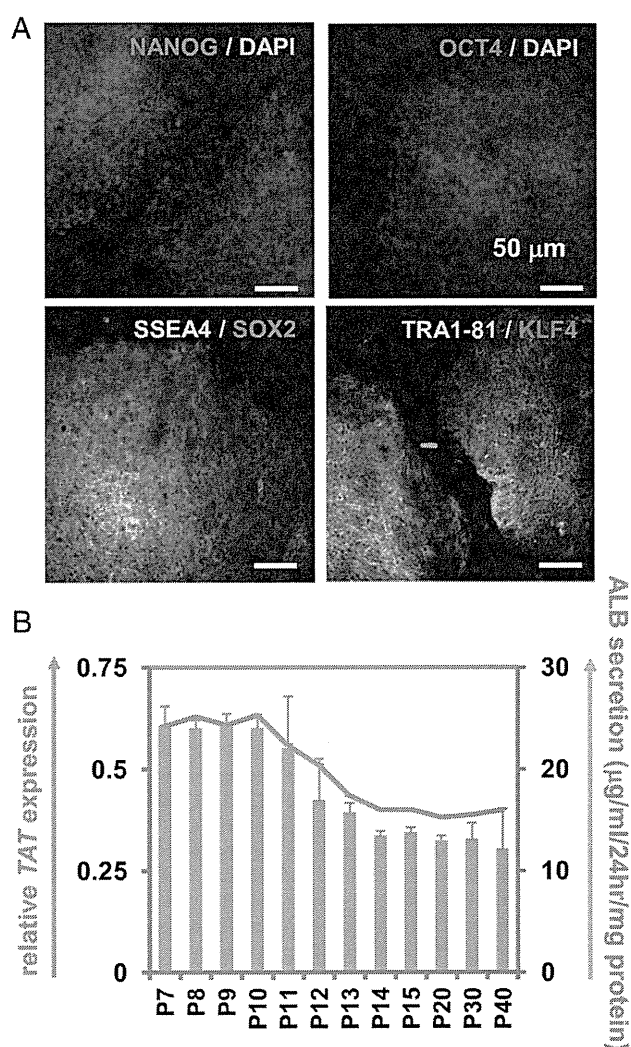


Fig. 1. Establishment and characterization of human iPSCs generated from PHHs. (A) The PHH-iPSCs were subjected to immunostaining with anti-NANOG (red), OCT4 (red), SSEA4 (green), SOX2 (red), TRA1-81 (green), and KLF4 (red) antibodies. Nuclei were counterstained with DAPI (blue) (*Upper*). (B) The TAT expression and ALB secretion levels in the PHH-iPS-HLCs (P7–P40) were examined. On the y axis, the gene expression level of TAT in PHHs was taken as 1.0.

the 12 donors, all of the PHH-iPSCs were differentiated into the HLCs as described in Fig. 2A. However, the differences in hepatic function among PHH-iPS-HLCs could not be properly compared because there were large inter-PHH-iPSC line differences in the hepatic differentiation efficiency based on ALB or asialoglycoprotein receptor 1 (ASGR1) expression analysis (Fig. 2B). In addition, there were also large inter-PHH-iPS-HLC line differences in ALB or urea secretion capacities (Fig. 2C). These results suggest that it is impossible to compare the hepatic characteristics among PHH-iPS-HLCs without compensating for the differences in the hepatic differentiation efficiency. Recently, we developed a method to maintain and proliferate the hepatoblast-like cells (HBCs) generated from human ESCs/iPSCs by using human laminin 111 (LN111) (10). To examine whether the hepatic differentiation efficiency could be made uniform by generating the HLCs following purification and proliferation of the HBCs, the PHH-iPS-HBCs were cultured on LN111 as

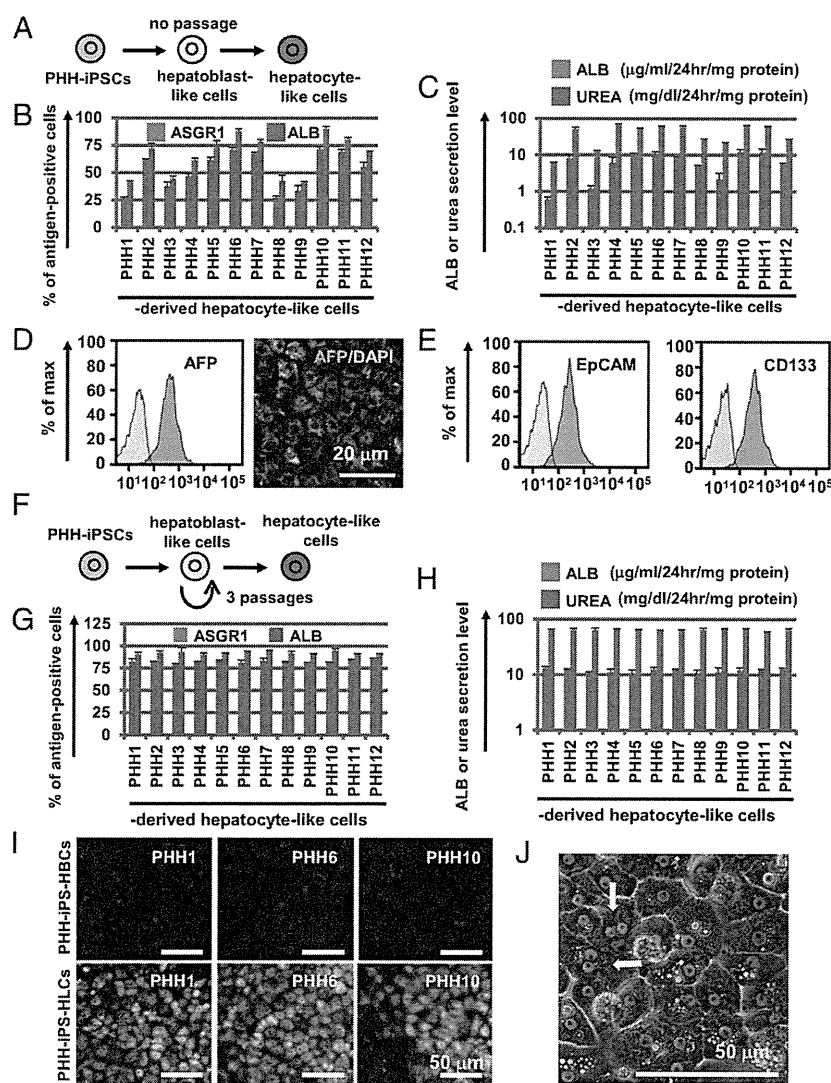


Fig. 2. Highly efficient hepatocyte differentiation from PHH-iPSCs independent of their differentiation tendency. (A) PHH-iPSCs were differentiated into the HLCs via the HBCs. (B) On day 25 of differentiation, the efficiency of hepatocyte differentiation was measured by estimating the percentage of ASGR1- or ALB-positive cells using FACS analysis. (C) The amount of ALB or urea secretion was examined in PHH-iPS-HLCs. (D) The percentage of AFP-positive cells in PHH-iPS-HLCs was examined by using FACS analysis (Left). The PHH-iPS-HLCs were subjected to immunostaining with anti-AFP (green) antibodies. Nuclei were counterstained with DAPI (blue) (Right). (E) The percentage of EpCAM- and CD133-positive cells in PHH-iPS-HLCs was examined by using FACS analysis (Left). (F) PHH-iPSCs were differentiated into the hepatic lineage, and then PHH-iPS-HLCs were purified and maintained for three passages on human LN111. Thereafter, expanded PHH-iPS-HLCs were differentiated into the HLCs. (G) The efficiency of hepatic differentiation from PHH-iPS-HLCs was measured by estimating the percentage of ASGR1- or ALB-positive cells using FACS analysis. (H) The amount of ALB or urea secretion in PHH-iPS-HLCs was examined. Data represent the mean \pm SD from three independent differentiations. (I) The PHH1-, 6-, or 10-iPS-HLCs and -HLCs were subjected to immunostaining with anti- α AT (green) antibodies. Nuclei were counterstained with DAPI (blue). (J) A phase-contrast micrograph of PHH-iPS-HLCs.

previously described (10), and then differentiated into the HLCs. Almost all of the cells were positive for the hepatoblast marker [alpha-fetoprotein (AFP)] (Fig. 2D). In addition, the PHH-iPS-HLCs were positive for two other hepatoblast markers, EpCAM and CD133 (Fig. 2E). To examine the hepatic differentiation efficiency of the PHH-iPS-HLCs maintained on LN111-coated dishes for three passages (Fig. 2F), the HLCs were differentiated into the HLCs, and then the percentage of ALB- and ASGR1-positive cells was measured by FACS analysis (Fig. 2G). All 12 PHH-iPS-HLCs could efficiently differentiate into the HLCs, yielding more than 75% or 85% ASGR1- or ALB-positive cells, respectively. In addition, there was little difference between the PHH-iPS lines in ALB or urea secretion capacities (Fig. 2H). Although there were large differences in the hepatic differentiation capacity among the PHH1/6/10 (Fig. 2B), PHH1/6/10-iPS-HLCs could efficiently differentiate into the HLCs that homogeneously expressed α AT (Fig. 2I). After the hepatic differentiation of the PHH-iPS-HLCs, the morphology of the HLCs was similar to that of the PHHs: polygonal with distinct round binuclei (Fig. 2J). These results indicated that the hepatic differentiation efficiency of the 12 PHH-iPS lines could be rendered uniform by inducing hepatic maturation after the establishment of self-renewing HBCs. Therefore, we expected

that differences in the hepatic characteristics among the HLCs generated from the 12 individual donor PHH-iPS-HLCs could be properly compared. In addition, the hepatic differentiation efficiency could be rendered uniform not only in the PHH-iPS lines but also in non-PHH-iPS lines and human ESCs by performing hepatic maturation after the establishment of self-renewing HBCs (*SI Appendix*, Fig. S4). In Figs. 3 and 4, the HLCs were differentiated after the HBC proliferation step to normalize the hepatic differentiation efficiency.

PHH-iPS-HLCs Retained Donor-Specific Drug Metabolism Capacity and Drug Responsiveness. To examine whether the hepatic functions of individual PHH-iPS-HLCs reflect those of individual PHHs, the CYP metabolism capacity and drug responsiveness of PHH-iPS-HLCs were compared with those of PHHs. PHHs are often used as a positive control to assess the hepatic functions of the HLCs, although in all of the previous reports, the donor of PHHs has been different from that of human iPSCs. Because it is generally considered that CYP activity differs widely among individuals, the hepatic functions of the HLCs should be compared with those of genetically identical PHHs to accurately evaluate the hepatic functions of the HLCs. The CYP1A2, -2C9, and -3A4 activity levels in the PHH-iPS-HLCs were ~60% of

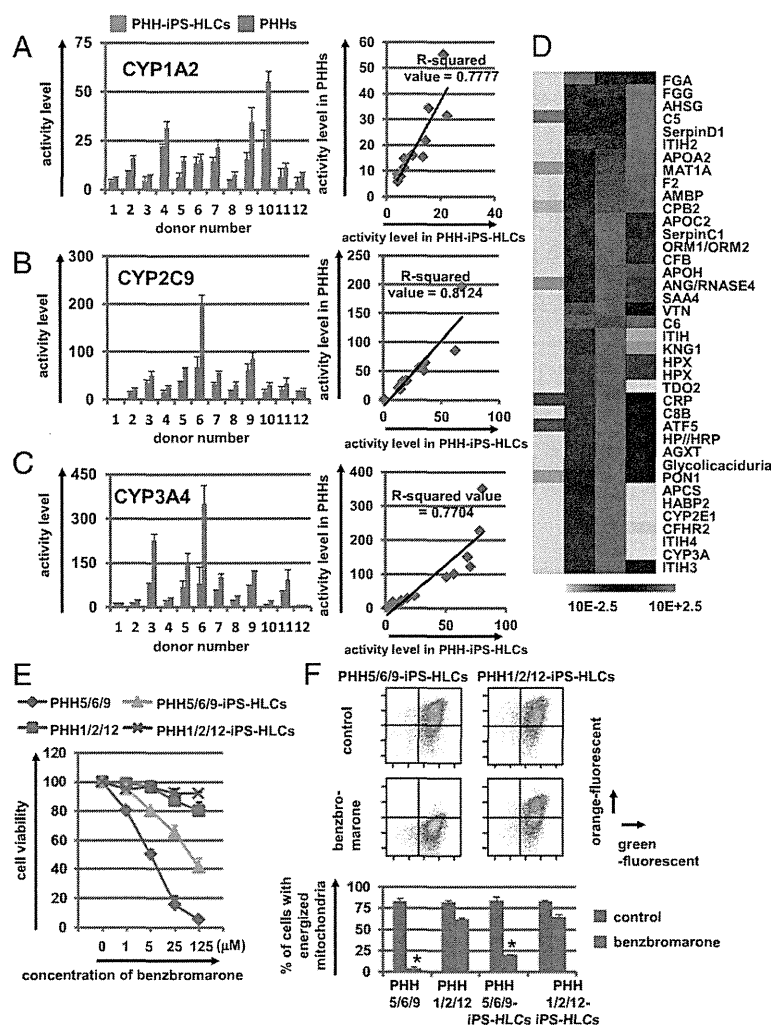


Fig. 3. The drug metabolism capacity and drug responsiveness of PHH-iPS-HLCs were highly correlated with those of their parental PHHs. (A–C) CYP1A2 (A), -2C9 (B), and -3A4 (C) activity levels in PHH-iPS-HLCs and PHHs were measured by LC-MS/MS analysis. The R-squared values are indicated in each figure. (D) The global gene expression analysis was performed in PHH9-iPSCs, PHH9-iPS-HLCs, PHH9s, and HepG2 (PHH-iPSCs, PHH-iPS-HLCs, and PHHs are genetically identical). Heat-map analyses of liver-specific genes are shown. (E) The cell viability of PHH5/6/9, PHH1/2/12, PHH5/6/9-iPS-HLCs, and PHH1/2/12-iPS-HLCs was examined after 24 h exposure to different concentrations of benzobromarone. The cell viability was expressed as a percentage of that in the cells treated only with solvent. (F) The percentage of cells with energized mitochondria in the DMSO-treated (control, *Upper*) or benzobromarone-treated (*Lower*) cells based on FACS analysis. Double-positive cells (green+/orange+) represent energized cells, whereas single-positive cells (green+/orange–) represent apoptotic and necrotic cells. Data represent the mean \pm SD from three independent experiments (*Lower Graph*). Student *t* test indicated that the percentages in the “control” were significantly higher than those in the “benzobromarone” group ($P < 0.01$). The “PHH5/6/9” represents the average value of cell viability (E) or mitochondrial membrane potential (F) in PHH5, PHH6, and PHH9. The “PHH1/2/12” represents the average value of cell viability or mitochondrial membrane potential in PHH1, PHH2, and PHH12. PHH5, PHH6, and PHH9 were the top three with respect to CYP2C9 activity levels, whereas PHH1, PHH2, and PHH12 had the lowest CYP2C9 activity levels.

those in the PHHs (Fig. 3 A–C and *SI Appendix*, Fig. S5). Interestingly, the CYP1A2, -2C9, and -3A4 activity levels in the PHH-iPS-HLCs were highly correlated with those in the PHHs (the R-squared values were more than 0.77) (Fig. 3 A, B, and C, respectively). These results suggest that it would be possible to predict the individual CYP activity levels through analysis of the CYP activity levels of the PHH-iPS-HLCs. Because the average and variance of CYP3A4 activity levels in PHH-iPS-HLCs, non-PHH-iPS-HLCs, and human ES-HLCs were similar to each other (*SI Appendix*, Fig. S6), the drug metabolism capacity of PHH-iPS-HLCs might be similar to that of nonliver tissue-derived iPS-HLCs and human ES-HLCs. Therefore, it might be possible to predict the diversity of drug metabolism capacity among donors by using nonliver tissue-derived iPS-HLCs and human ES-HLCs as well as PHH-iPS-HLCs. On the other hand, the CYP induction capacities of PHH-iPS-HLCs were weakly correlated with those of PHHs (*SI Appendix*, Fig. S7 A–C). To further investigate the characteristics of the HLCs, DNA microarray analyses were performed in genetically identical undifferentiated iPSCs, PHH-iPS-HLCs, and PHHs. The gene expression patterns of liver-specific genes, CYPs, and transporters in the PHH-iPS-HLCs were similar to those in PHHs (Fig. 3D and *SI Appendix*, Fig. S7 D and E, respectively). Next, the hepatotoxic drug responsiveness of PHH-iPS-HLCs was compared with that of PHHs. Benzobromarone, which is known to cause

hepatotoxicity by CYP2C9 metabolism (11), was treated to PHH5/6/9 and PHH5/6/9-iPS-HLCs, which have high CYP2C9 activity, or PHH1/2/12 and PHH1/2/12-iPS-HLCs which have low CYP2C9 activity (Fig. 3E). The susceptibility of the PHH5/6/9 and PHH5/6/9-iPS-HLCs to benzobromarone was higher than that of PHH1/2/12 and PHH1/2/12-iPS-HLCs, respectively. These results were attributed to the higher CYP2C9 activity levels in PHH5/6/9 and PHH5/6/9-iPS-HLCs compared with those in PHH1/2/12 and PHH1/2/12-iPS-HLCs. Because it is also known that benzobromarone causes mitochondrial toxicity (12), an assay of mitochondrial membrane potential was performed in benzobromarone-treated PHHs and PHH-iPS-HLCs (Fig. 3F). The mitochondrial toxicity observed in PHH5/6/9 and PHH5/6/9-iPS-HLCs was more severe than that in PHH1/2/12 and PHH1/2/12-iPS-HLCs, respectively. Taken together, these results suggest that the hepatic functions of the individual PHH-iPS-HLCs were highly correlated with those of individual PHHs.

Interindividual Differences in CYP2D6-Mediated Metabolism and Drug Toxicity, Which Are Caused by SNPs in CYP2D6, Are Reproduced in the PHH-iPS-HLCs. Because certain SNPs are known to have a large impact on CYP activity, the genetic variability of CYP plays an important role in interindividual differences in drug response. CYP2D6 shows the large phenotypic variability due to genetic polymorphism (13). We next examined whether the PHHs used

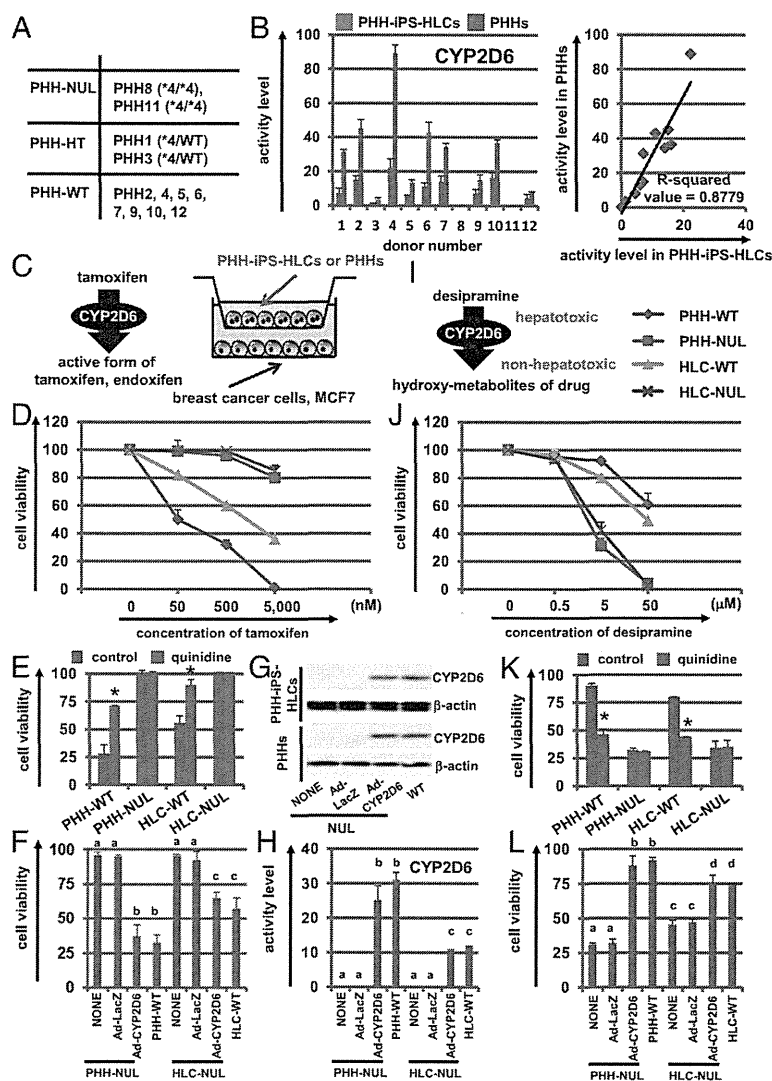


Fig. 4. The interindividual differences in CYP2D6 metabolism capacity and drug responsiveness induced by SNPs in CYP2D6 are reproduced in the PHH-iPS-HLCs. (A) SNPs (CYP2D6*3, *4, *5, *6, *7, *8, *16, and *21) in the CYP2D6 gene were analyzed. (B) The CYP2D6 activity levels in PHH-iPS-HLCs and PHHs were measured by LC-MS/MS analysis. (C) The pharmacological activity of tamoxifen-dependent conversion to its metabolite, endoxifen, by the CYP2D6. The coculture system of breast cancer cells (MCF-7 cells) and the PHH-iPS-HLCs are illustrated. (D) The cell viability of MCF-7 cells was assessed after 72-h exposure to different concentrations of tamoxifen. (E) The cell viability of MCF-7 cells, which were cocultured with PHH-WT, PHH-NUL, HLC-WT, and HLC-NUL, was assessed after 72-h exposure to 500 nM of tamoxifen in the presence or absence of 3 nM quinidine (a CYP2D6 inhibitor). (F) The cell viability of MCF-7 cells cocultured with Ad-CYP2D6-transduced PHH-NUL and HLC-NUL was examined after 72-h exposure to 500 nM of tamoxifen. (G and H) The CYP2D6 expression (G) and activity (H) levels in Ad-CYP2D6-transduced PHH-NUL and HLC-NUL were examined by Western blotting and LC-MS/MS analysis. (I) The detoxification of desipramine-dependent conversion to its conjugated form by the CYP2D6. (J) The cell viability of PHH-WT, PHH-NUL, HLC-WT, and HLC-NUL was assessed after 24-h exposure to different concentrations of desipramine. (K) The cell viability of the PHH-WT and HLC-WT was assessed after 24-h exposure to 5 μM of desipramine in the presence or absence of 5 μM of quinidine (a CYP2D6 inhibitor). (L) The cell viability of the Ad-CYP2D6-transduced PHH-NUL and HLC-NUL was examined after 24-h exposure to 5 μM of desipramine. The cell viability was expressed as a percentage of that in the cells treated with only solvent. Data represent the mean ± SD from three independent experiments. In E and K, Student t test indicated that the cell viability in the "control" was significantly higher than that in the "quinidine" group ($P < 0.01$). In F, H, and L, statistical significance was evaluated by ANOVA followed by Bonferroni post hoc tests to compare all groups. Groups that do not share the same letter are significantly different from each other ($P < 0.05$).

in this study have the CYP2D6 poor metabolizer genotypes (CYP2D6*3, *4, *5, *6, *7, *8, *16, and *21) (5). PHH8 and -11 have CYP2D6*4 (null allele), whereas the others have a wild type (WT) or hetero allele (SI Appendix, Table S3 and Fig. 4A). Consistent with this finding, the PHH8/11-iPS-HLCs also have CYP2D6*4, whereas the others have a wild type or hetero allele. As expected, the CYP2D6 activity levels in the PHH8/11 (PHH-NUL) and PHH8/11-iPS-HLC (HLC-NUL) were significantly lower than those in the PHH-WT and HLC-WT, respectively (Fig. 4B). The pharmacological activity of tamoxifen, which is the most widely used agent for patients with breast cancer, is dependent on its conversion to its metabolite, endoxifen, by the CYP2D6 (Fig. 4C). To examine whether the pharmacological activity of tamoxifen could be predicted by using PHHs and HLCs that have either the null type CYP2D6*4 allele or wild-type CYP2D6 allele, the breast cancer cell line MCF7 was cocultured with PHHs or HLCs, and then the cells were treated with tamoxifen (Fig. 4D). The cell viability of MCF7 cells cocultured with PHHs-NUL or HLCs-NUL was significantly higher than that of MCF7 cells cocultured with PHHs-WT or HLCs-WT. The decrease in cell viability of MCF7 cells cocultured with PHHs-WT or HLCs-WT was rescued by treatment with a CYP2D6 inhibitor, quinidine (Fig. 4E). We also

confirmed that the cell viability of MCF7 cells cocultured with PHHs-NUL or HLCs-NUL was decreased by CYP2D6 overexpression in the PHHs-NUL or HLCs-NUL (Fig. 4F). Note that the expression (Fig. 4G) and activity (Fig. 4H) levels of CYP2D6 in CYP2D6-expressing adenovirus vector (Ad-CYP2D6)-transduced PHHs-NUL or HLCs-NUL were comparable to those of PHHs-WT or HLCs-WT. These results indicated that the PHHs-WT and HLCs-WT could more efficiently metabolize tamoxifen than the PHHs-NUL and HLCs-NUL, respectively, and thereby induced higher toxicity in MCF7 cells. Similar results were obtained with the other breast cancer cell line, T-47D (SI Appendix, Fig. S8 A–D). Next, we examined whether the CYP2D6-mediated drug-induced hepatotoxicity could be predicted by using PHHs and HLCs having either a null type CYP2D6*4 allele or wild-type CYP2D6 allele. PHHs and HLCs were treated with desipramine, which is known to cause hepatotoxicity (Fig. 4I) (14). The cell viability of PHHs-NUL and HLCs-NUL was significantly lower than that of PHHs-WT and HLCs-WT (Fig. 4J). The cell viability of the PHHs-WT or HLCs-WT was decreased by treatment with a CYP2D6 inhibitor, quinidine (Fig. 4K). We also confirmed that the decrease in the cell viability of the PHHs-NUL or HLCs-NUL was rescued by CYP2D6 overexpression in the PHHs-NUL or HLCs-NUL (Fig. 4L). Similar

results were obtained with the other hepatotoxic drug, perhexiline (*SI Appendix*, Fig. S8 E–H). These results indicated that the PHHs-WT and HLCs-WT could more efficiently metabolize imipramine and thereby reduce toxicity compared with the PHHs-NUL and HLCs-NUL. Taken together, our findings showed that the interindividual differences in CYP metabolism capacity and drug responsiveness, which are prescribed by an SNP in genes encoding CYPs, were also reproduced in the PHH-iPS-HLCs.

Discussion

The purpose of this study was to examine whether the individual HLCs could reproduce the hepatic function of individual PHHs. A Yamanaka 4 factor-expressing SeV vector was used in this study to generate integration-free human iPSCs from PHHs. It is known that SeV vectors can express exogenous genes without chromosomal insertion, because these vectors replicate their genomes exclusively in the cytoplasm (15). To examine the different cellular phenotypes associated with SNPs in human iPSC derivatives, the use of integration-free human iPSCs is essential.

We found that the CYP activity levels of the PHH-iPS-HLCs reflected those of parent PHHs, as shown in Fig. 3 A–C. There were few interindividual differences in the ratio of CYP expression levels in the PHH-iPS-HLCs to those in PHHs (*SI Appendix*, Fig. S5). Together, these results suggest that it is possible to predict the individual CYP activity levels through analysis of the CYP activity levels of the PHH-iPS-HLCs. In the future, it will be necessary to confirm these results in skin or blood cell-derived iPSCs as well as PHH-iPSCs, although donor-matched PHHs and blood cells (or skin cells) are difficult to obtain. In addition, the comparison of hepatic functions between genetically identical PHHs and PHH-iPS-HLCs (Fig. 3 A–C) would enable us to accurately ascertain whether the HLCs exhibit sufficient hepatic function to be a suitable substitute for PHHs in the early phase of pharmaceutical development. Because the drug responsiveness of the individual HLCs reflected that of individual PHHs (Fig. 3 E and F), it might be possible to perform personalized drug therapy following drug screening using a patient's HLCs. However, the R-squared values of the individual CYP activities differed from each other (Fig. 3 A–C), suggesting that the activity levels of some CYPs are largely

influenced not only by genetic information but also by environmental factors, such as dietary or smoking habits.

The interindividual differences of CYP2D6 metabolism capacity and drug responsiveness that were prescribed by SNP in genes encoding CYP2D6 were reproduced in the PHH-iPS-HLCs (Fig. 4). It was impossible to perform drug screening in the human hepatocytes derived from a donor with rare SNPs because these hepatocytes could not be obtained. However, because human iPSCs can be generated from such donors with rare SNPs, the CYP metabolism capacity and drug responsiveness of these donors might be possible to predict. Further, it would also be possible to identify the novel SNP responsible for an unexpected hepatotoxicity by using the HLCs in which whole genome sequences are known. We thus believe that the HLCs will be a powerful tool not only for accurate and efficient drug development but also for personalized drug therapy.

Experimental Procedures

DNA Microarray. Total RNA was prepared from the PHH9-iPSCs, PHH9-iPS-HLCs, PHH9, and human hepatocellular carcinoma cell lines by using an RNeasy Mini kit. A pool of three independent samples was used in this study. cRNA amplifying, labeling, hybridizing, and analyzing were performed at Milltenyi Biotec. The Gene Expression Omnibus (GEO) accession no. for the microarray analysis is GSE61287.

Flow Cytometry. Single-cell suspensions of human iPSC-derived cells were fixed with 2% (vol/vol) paraformaldehyde (PFA) for 20 min, and then incubated with the primary antibody (described in *SI Appendix*, Table S1), followed by the secondary antibody (described in *SI Appendix*, Table S2). In case of the intracellular staining, the Permeabilization Buffer (eBioscience) was used to create holes in the membrane thereby allowing the antibodies to enter the cell effectively. Flow cytometry analysis was performed using a FACS LSR Fortessa flow cytometer (BD Biosciences).

ACKNOWLEDGMENTS. We thank Yasuko Hagihara, Natsumi Mimura, and Shigemitsu Ioyama for their excellent technical support. H.M. and K.K. were supported by grants from the Ministry of Health, Labor, and Welfare. H.M. was also supported by the Project for Technological Development, Research Center Network for Realization of Regenerative Medicine of the Japan Science and Technology Agency and by the Uehara Memorial Foundation. F.S. was supported by the Program for Promotion of Fundamental Studies in Health Sciences of the National Institute of Biomedical Innovation. K.T. and Y.N. were supported by a grant-in-aid for the Japan Society for the Promotion of Science Fellows.

1. Takayama K, et al. (2012) Efficient generation of functional hepatocytes from human embryonic stem cells and induced pluripotent stem cells by HNF4 α transduction. *Mol Ther* 20(1):127–137.
2. Medine CN, et al. (2013) Developing high-fidelity hepatotoxicity models from pluripotent stem cells. *Stem Cells Transl Med* 2(7):505–509.
3. Ingelman-Sundberg M (2004) Pharmacogenetics of cytochrome P450 and its applications in drug therapy: The past, present and future. *Trends Pharmacol Sci* 25(4):193–200.
4. Ingelman-Sundberg M (2001) Genetic susceptibility to adverse effects of drugs and environmental toxicants. The role of the CYP family of enzymes. *Mutat Res* 482(1–2):11–19.
5. Zhou SF (2009) Polymorphism of human cytochrome P450 2D6 and its clinical significance: Part I. *Clin Pharmacokinet* 48(11):689–723.
6. Borges S, et al. (2006) Quantitative effect of CYP2D6 genotype and inhibitors on tamoxifen metabolism: Implication for optimization of breast cancer treatment. *Clin Pharmacol Ther* 80(1):61–74.
7. Bakke OM, Manocchia M, de Abajo F, Kaitin KI, Lasagna L (1995) Drug safety discontinuations in the United Kingdom, the United States, and Spain from 1974 through 1993: A regulatory perspective. *Clin Pharmacol Ther* 58(1):108–117.
8. Lin T, et al. (2009) A chemical platform for improved induction of human iPSCs. *Nat Methods* 6(11):805–808.
9. Polo JM, et al. (2010) Cell type of origin influences the molecular and functional properties of mouse induced pluripotent stem cells. *Nat Biotechnol* 28(8):848–855.
10. Takayama K, et al. (2013) Long-term self-renewal of human ES/iPS-derived hepatoblast-like cells on human laminin 111-coated dishes. *Stem Cell Reports* 1(4):322–335.
11. McDonald MG, Rettie AE (2007) Sequential metabolism and bioactivation of the hepatotoxin benzobromarone: Formation of glutathione adducts from a catechol intermediate. *Chem Res Toxicol* 20(12):1833–1842.
12. Kaufmann P, et al. (2005) Mechanisms of benzarone and benzobromarone-induced hepatic toxicity. *Hepatology* 41(4):925–935.
13. Ingelman-Sundberg M (2005) Genetic polymorphisms of cytochrome P450 2D6 (CYP2D6): Clinical consequences, evolutionary aspects and functional diversity. *Pharmacogenomics J* 5(1):6–13.
14. Spina E, et al. (1997) Relationship between plasma desipramine levels, CYP2D6 phenotype and clinical response to desipramine: A prospective study. *Eur J Clin Pharmacol* 51(5):395–398.
15. Nishimura K, et al. (2011) Development of defective and persistent Sendai virus vector: A unique gene delivery/expression system ideal for cell reprogramming. *J Biol Chem* 286(6):4760–4771.

①-4

進行性家族性肝内胆汁うっ滞症 2 型の疾患モデル—iPS 細胞由来分化誘導肝細胞を用いた解析—

今川 和生¹⁾, 谷川 健²⁾, 新開 真人³⁾, 鹿毛 政義²⁾,
須磨崎 亮¹⁾

筑波大学 医学医療系 小児科¹⁾,
久留米大学病院病理部²⁾,
神奈川県立こども医療センター外科³⁾

【目的】進行性家族性肝内胆汁うっ滞症 (PFIC) 2 型は, 胆汁酸トランスポーター (BSEP; bile salt export pump) に異常があり, 多くの患児で生体肝移植を必要とすることから新規治療薬の開発が望まれている。しかしながら, BSEP ノックアウトマウスでは肝障害が軽度でヒトと表現型が異なることが知られている。そこで, 疾患解析や創薬研究に応用出来る PFIC2 型のモデル開発を目的に BSEP 欠損患者から iPS 細胞を作製し, 分化誘導肝細胞 (HLC; hepatocyte-like cell) を解析した。

【対象と方法】<症例 1>3 カ月時に遷延性黄疸のために紹介された。γ GTP 正常の胆汁うっ滞と肝組織所見での BSEP 陰性から PFIC2 型が疑われたが, BSEP exon 解析で変異なく, normal-γ GTP PFIC と診断された。8 カ月時に生体肝移植が行われ, 以後胆汁うっ滞の再燃や肝外症状なし。<症例 2>2 カ月時に γ GTP 正常の胆汁うっ滞に気づかれ, BSEP exon 解析で複合ヘテロ変異 (-24C>A, 2417G>A) を同定され, PFIC2 型と診断された。2 歳 8 カ月時に生体肝移植が行われた。摘出肝で BSEP 減弱の所見あり。対象患者 2 名の血液細胞から iPS 細胞を樹立した。液性因子を分化段階特異的に作用させ, HLC を分化誘導した。【結果】iPS 細胞は Nanog などの未分化マーカーを発現し, 多分化能を示した。分化 25 日目の HLC はアルブミンを発現しており, 電子顕微鏡観察で微細胆管構造を示した。BSEP 免疫蛍光染色で細胞膜上の染色が認められなかった。また, 蛍光胆汁排泄試薬 CLF を用いたアッセイでは, 胆汁排泄能の低下が認められた。これらの結果は PFIC2 型の主病態である, BSEP 発現低下と胆汁排泄能低下を再現していると考えられた。特に症例 1 は BSEP の発現と蛋白合成に異常なく, 細胞膜への輸送障害, 症例 2 は BSEP の輸送障害+構造異常が本態である可能性が示唆された。【結語】BSEP 欠損患者から作製した iPS 細胞由来分化誘導肝細胞は, PFIC2 型の病態を再現し得ると考えられた。

O-21 進行性家族性肝内胆汁うっ滞症2型の組織および免疫組織化学所見の多彩性について

○谷川 健¹, 鹿毛政義¹, 杉浦時雄², 今川和生³, 須磨崎亮³, 近藤礼一郎⁴, 中山正道⁴, 草野弘宣⁴, 真田咲子⁴, 秋葉 純⁴, 小笠原幸子⁴, 矢野博久⁴
久留米大学病院病理診断科・病理部¹, 名古屋市立大学小児科², 筑波大学小児科³, 久留米大学医学部病理学講座⁴

【背景】進行性家族性肝内胆汁うっ滞症2型(以下PFIC2)は肝トランスporter-BSEPの欠損により,胆汁うっ滞をきたす遺伝性疾患である。PFIC2の診断は遺伝子診断で確定される。しかし,PFIC2が疑われるすべての症例に遺伝子検査が施行できるわけではない。PFIC2の遺伝子検査適応を決める上で,肝生検は有用である。なぜなら,PFIC2の組織形態には,小葉全体にわたる肝細胞巨細胞性変化,小葉および門脈域の炎症細胞浸潤および線維化という特徴があり,免疫組織化学でBSEP発現が陰性であるからである。しかしながら,PFIC2と遺伝子診断された症例でも非典型的な組織所見を示す症例やBSEP発現が認められる症例があり,病理学的に不明な点がある。

【目的】遺伝子診断されたPFIC2症例の組織所見および免疫組織化学所見を検討し,その病理像を明確にする。

【方法】遺伝子診断されたPFIC2患者8症例(年齢は4ヶ月~6歳6ヶ月,男性4症例,女性4症例,移植例が6症例,生検が2症例)を対象とし,肝組織形態所見,肝トランスporter-免疫組織化学所見(BSEP,MDR3,MRP2,MRP3)を検討した。

【成績】8症例中5症例は上記の典型的な組織形態所見を示した。その他の3例はPFIC1型に類似した組織所見を呈した。すなわち,小葉構築はほぼ保たれており,門脈域の線維化はごく軽度,薄い線維性架橋形成,門脈域および小葉の炎症所見がごく軽度,肝細胞巨細胞性変化はほとんどなく,小型肝細胞の敷石状配列あるいは腺房様配列を示した。典型的な組織形態所見を示した5症例はBSEP免疫組織化学発現が陰性であった。非典型的な組織形態所見を示した3症例のBSEP免疫組織化学発現は2症例が陰性であり,1症例は発現が見られ,不規則に減弱,消失していた。MRP2は組織形態典型例3症例および非典型例2症例に施行し,5症例とも全体的に発現が増強していた。MDR3,MRP3は組織形態非典型例1症例に施行し,どちらも全体的に発現が増強していた。

【考案】PFIC2でありながらPFIC1に類似する組織形態変化の成因,BSEP発現の原因と機序は不明である。MDR3,MRP2,MRP3の発現増強はBSEP傷害による代償性変化と考えられる。

【結語】PFIC2遺伝子診断のスクリーニングには肝生検およびBSEP免疫組織化学が有用であるが,PFIC2は多彩な組織所見を示すことやBSEP発現が認められる症例があることを念頭に置くべきである。

★O-24 進行性家族性肝内胆汁うっ滞症2型のiPS細胞由来分化誘導肝細胞を用いた病態再現とフェニル酪酸の薬効評価

○今川和生¹, 谷川 健², 鹿毛政義³, 須磨崎亮⁴
筑波大学医学医療系小児科¹, 久留米大学病院病理部²

【目的】進行性家族性肝内胆汁うっ滞症(PFIC; progressive familial intrahepatic cholestasis)2型は,胆汁酸トランスporter(BSEP; bile salt export pump)の異常により,重篤な胆汁うっ滞性肝障害を起こし,救命のためにしばしば肝移植を要する。しかしながら,BSEPノックアウトマウスでは肝障害が軽度であることから,PFIC2型の病態を反映した本疾患の解析や創薬研究に応用可能なヒト疾患モデルの構築が期待されている。そこで,PFIC2型の新規疾患モデルと薬効評価系の創製を目的に,同症患者からiPS細胞を作製し,分化誘導肝細胞(iPS-HLC; iPS-derived hepatocyte-like cells)の解析を行った。

【方法】PFIC2型患者2名の血液細胞から山中4因子搭載センダイウイルスベクターを用いてiPS細胞を樹立し,リアルタイムPCRや免疫蛍光染色で未分化マーカーの発現を確認すると共に,胚様体形成で三胚葉への分化能を調べた。これらの樹立したiPS細胞からiPS-HLCを分化誘導し,免疫蛍光染色やbiliary excretion index (BEI) アッセイによりPFIC2型の病態を再現し得るか否かを検討した。さらに,iPS-HLCにフェニル酪酸を作用させ,その薬効を免疫蛍光染色やBEIアッセイにより評価した。

【結果・考察】PFIC2型患者より樹立したiPS細胞はOCT4やNANOGの未分化マーカーを発現し,胚様体形成で三胚葉への分化能を示した。PFIC2型iPS-HLCでは細胞膜上BSEP発現が消失し,BEIは健常者iPS-HLCに比して低値を示し,胆汁排泄能が低下していると考えられた。フェニル酪酸を作用させたPFIC2型iPS-HLCでは,非作用群と比較して細胞膜上BSEPが強く発現し,BEI値は上昇した。したがって,フェニル酪酸のPFIC2型に対する薬効であるBSEP発現改善作用と胆汁排泄能改善作用を,PFIC2型iPS-HLCを用いて再現し得ると考えられた。

【結語】PFIC2型iPS-HLCはPFIC2型の主要病態を再現し,新規疾患モデルおよび薬効評価系として有用であることが示唆された。

RESEARCH

Open Access



In vivo hepatogenic capacity and therapeutic potential of stem cells from human exfoliated deciduous teeth in liver fibrosis in mice

Takayoshi Yamaza^{1†}, Fatima Safira Alatas^{2†}, Ratih Yuniartha², Haruyoshi Yamaza³, Junko K. Fujiyoshi⁴, Yusuke Yanagi², Koichiro Yoshimaru², Makoto Hayashida², Toshiharu Matsuura², Reona Aijima¹, Kenji Ihara⁵, Shouichi Ohga⁶, Songtao Shi⁷, Kazuaki Nonaka³ and Tomoaki Taguchi^{2*}

Abstract

Introduction: Liver transplantation is a gold standard treatment for intractable liver diseases. Because of the shortage of donor organs, alternative therapies have been required. Due to their potential to differentiate into a variety of mature cells, stem cells are considered feasible cell sources for liver regeneration. Stem cells from human exfoliated deciduous teeth (SHED) exhibit hepatogenic capability *in vitro*. In this study, we investigated their *in vivo* capabilities of homing and hepatocyte differentiation and therapeutic efficacy for liver disorders in carbon tetrachloride (CCl₄)-induced liver fibrosis model mice.

Methods: We transplanted SHED into CCl₄-induced liver fibrosis model mice through the spleen, and analyzed the *in vivo* homing and therapeutic effects by optical, biochemical, histological, immunological and molecular biological assays. We then sorted human leukocyte antigen-ABC (HLA-ABC)-positive cells from primary CCl₄-damaged recipient livers, and analyzed their fusogenicity and hepatic characteristics by flow cytometric, genomic DNA, hepatocyte-specific gene assays. Furthermore, we examined the treatment effects of HLA-positive cells to a hepatic dysfunction by a secondary transplantation into CCl₄-treated mice.

Results: Transplanted SHED homed to recipient livers, and expressed HLA-ABC, human hepatocyte specific antigen hepatocyte paraffin 1 and human albumin. SHED transplantation markedly recovered liver dysfunction and led to anti-fibrotic and anti-inflammatory effects in the recipient livers. SHED-derived HLA-ABC-positive cells that were sorted from the primary recipient liver tissues with CCl₄ damage did not fuse with the host mouse liver cells. Sorted HLA-positive cells not only expressed human hepatocyte-specific genes including albumin, cytochrome P450 1A1, fumarylacetoacetase, tyrosine aminotransferase, uridine 5'-diphospho-glucuronosyltransferase, transferrin and transthyretin, but also secreted human albumin, urea and blood urea nitrogen. Furthermore, SHED-derived HLA-ABC-positive cells were secondary transplanted into CCl₄-treated mice. The donor cells homed into secondary recipient livers, and expressed hepatocyte paraffin 1 and human albumin, as well as HLA-ABC. The secondary transplantation recovered a liver dysfunction in secondary recipients.

Conclusions: This study indicates that transplanted SHED improve hepatic dysfunction and directly transform into hepatocytes without cell fusion in CCl₄-treated mice, suggesting that SHED may provide a feasible cell source for liver regeneration.

* Correspondence: taguchi@ped surg.med.kyushu-u.ac.jp

[†]Equal contributors

²Department of Pediatric Surgery, Kyushu University Graduate School of Medical Sciences, 3-1-1 Maidashi, Higashi-ku, Fukuoka 812-8582, Japan
Full list of author information is available at the end of the article



© 2015 Yamaza et al. **Open Access** This article is distributed under the terms of the Creative Commons Attribution 4.0 International License (<http://creativecommons.org/licenses/by/4.0/>), which permits unrestricted use, distribution, and reproduction in any medium, provided you give appropriate credit to the original author(s) and the source, provide a link to the Creative Commons license, and indicate if changes were made. The Creative Commons Public Domain Dedication waiver (<http://creativecommons.org/publicdomain/zero/1.0/>) applies to the data made available in this article, unless otherwise stated.

Introduction

Hepatic fibrosis is a severe chronic condition that occurs as a result of various congenital and acquired hepatic disorders, including viral, drug-induced, cholestatic, metabolic, and autoimmune diseases. Cirrhosis, the most advanced stage of hepatic fibrosis, usually progresses to hepatocellular carcinoma, resulting in liver failure without the liver's usual self-regenerative capability. Unfortunately, current pharmaceutical and immunological treatments are unable to cure patients with hepatic fibrosis and/or cirrhosis. Liver transplantation is therefore the only treatment with clinical success. However, few patients benefit from organ grafting because of high medical expenses, the long-term wait for a donor liver, organ rejection, and complications [1]. Hepatocyte transplantation as an alternative is also associated with a limited cell supply and minimal engraft efficacy [2]. Another alternative therapy is therefore required urgently for hepatic fibrosis and/or cirrhosis. A concept of stem cell-based tissue engineering and regenerative medicine is expected to provide novel and promising therapeutics for refractory liver diseases [3].

Human mesenchymal stem cells (MSCs) exhibit self-renewal and multipotency into a variety of mature cells, including hepatocytes [4]. Human MSCs have been identified in a variety of human tissues, including bone marrow [5], adipose tissue [6], umbilical cord blood [7], amniotic fluid stem cells [8], and dental pulp tissue [9]. Recent studies also evaluate immunomodulatory effects of MSCs [10]. MSCs are therefore considered a feasible cell source for tissue engineering and regenerative medicine [11]. Some clinical phase I, I/II, and II trials have demonstrated that human MSC transplantation recovers hepatic function in liver cirrhosis patients [12–14], indicating that human MSCs might be a promising candidate for treatments of liver dysfunction.

Stem cells from human exfoliated deciduous teeth (SHED) are a major focus area in tissue engineering and regenerative medicine. SHED are discovered in remnant dental pulp tissues of human exfoliated deciduous teeth, and share MSC characteristics, including fibroblastic features, clonogenicity, cell surface antigen expression, cell proliferative capacity, and multidifferentiation potency [15]. SHED also modulate immune responses of interleukin-17-producing helper T (Th17) cells, regulatory T cells (Tregs), and dendritic cells [16, 17]. Recent studies have evaluated the latent potential of SHED in tissue engineering for bone regeneration [18, 19] and cell-based therapy for a variety of refractory systemic diseases, including systemic lupus erythematosus, spinal cord injury, Parkinson's disease, and diabetes [16, 20–22]. Furthermore, cryopreservation of dental pulp tissues from human deciduous teeth has succeeded [23].

Accumulating evidence has demonstrated that a variety of human MSCs, including bone marrow-derived,

adipose tissue-derived, umbilical cord blood-derived, and Wharton's jelly-derived MSCs, are capable of differentiating into hepatocyte-like cells *in vivo* in animal models of hepatic failure [24–26]. Advanced tissue engineering techniques accelerate a transdifferentiation ability of human MSCs into hepatocytes [27, 28]. In comparison with other human tissues, exfoliated deciduous teeth offer significant advantages of less ethical controversies and readily accessible source, easy and minimally invasive collection, and retain high stem cell potential such as cell proliferation, multipotency, and immunomodulatory functions [14–16], even after cryopreservation [23]. Recently, many investigators have investigated a SHED bank for allogenic cell therapy, as well as autologous cell therapy [23, 29, 30]. Exfoliated deciduous teeth might therefore be a feasible cell source for MSC-based therapy for both pediatric and adult patients with liver dysfunction.

Although SHED are known to be capable of differentiating into hepatocyte-like cells *in vitro* [31], they have not been evaluated for their *in vivo* hepatogenic capacity or therapeutic efficacy in liver disorders. In this study, we reveal that SHED transplantation recovers the liver dysfunction of carbon tetrachloride (CCl₄)-treated mice. The engrafted SHED convert directly into human hepatocyte-like cells without fusion in fibrous livers of CCl₄-treated mice. Furthermore, these *in vivo* SHED-converted hepatocyte-like cells participate in the hepatic recovery via both direct (tissue replacement) and indirect (anti-fibrotic and anti-inflammatory effects) integration in CCl₄-injured mouse livers.

Methods

Ethics statement and human subjects

Human samples were collected as discarded biological/clinical samples from healthy pediatric donors (5–7 years old) in the Department of Pediatric Dentistry of Kyushu University Hospital, Fukuoka, Japan. Procedures using human samples were conducted in accordance with Declaration of Helsinki, and were approved by Kyushu University Institutional Review Board for Human Genome/Gene Research (Protocol Number: 393-01). Written informed consent was obtained from each parent on behalf of the child donors. All animal experiments were approved by Institutional Animal Care and Use Committee of Kyushu University (Protocol Number: A21-044-1).

Isolation and culture of SHED

Isolation and culture of SHED were performed according to our previous reports [16, 23]. The detailed method is described in Additional file 1. To confirm whether our isolated cells were MSCs, the obtained passage 3 (P3) cells were assessed by a flow cytometric analysis as described

previously [16]. The P3 cells were also cultured under osteogenic, chondrogenic, and adipogenic conditions as described previously [23]. The P3 cells were positive for CD146, CD73, CD105, and CD90, but negative for hematopoietic markers (CD34, CD45, CD14, and CD11b) (Figure S1A in Additional file 2). The P3 cells also exhibited multipotency into three types of classical mesenchymal lineage cells (Figure S1B–G in Additional file 2). These phenotypes indicated that our isolated SHED fulfilled minimal and standard criteria for MSCs [32]. The P3 cells were therefore used for further experiments in this study.

Chronic liver fibrosis model in mice

A mixture of CCl₄ (0.5 ml/kg body weight; Wako Pure Chemicals, Osaka, Japan) and olive oil (1:4 volume/volume; Wako Pure Chemicals) was injected intraperitoneally into C57BL/6J mice (male, 8 weeks old; Kyudo, Tosu, Japan) twice a week during this experimental period (see Fig. 1a).

Age-matched and sex-matched mice injected with olive oil (Wako Pure Chemicals) were used as controls for primary (*n* = 5) and secondary (*n* = 5) transplantation.

Primary transplantation of SHED

One million SHED (P3) suspended in 100 μl phosphate-buffered saline (PBS) were intrasplenically transplanted into mice treated with CCl₄ for 4 weeks (*n* = 5) (Fig. 1a). As a control, 100 μl PBS were infused intrasplenically into mice treated with CCl₄ for 4 weeks (*n* = 5). The mice continuously received CCl₄ twice a week for an additional 4-week treatment after the transplantation. All of the animals were sacrificed to harvest the livers and peripheral blood.

Colorimetric analysis and enzyme-linked immunosorbent assay of mouse serum and liver samples

Serum alkaline phosphatase (ALP), alanine aminotransferase (ALT), aspartate aminotransferase (AST), and total

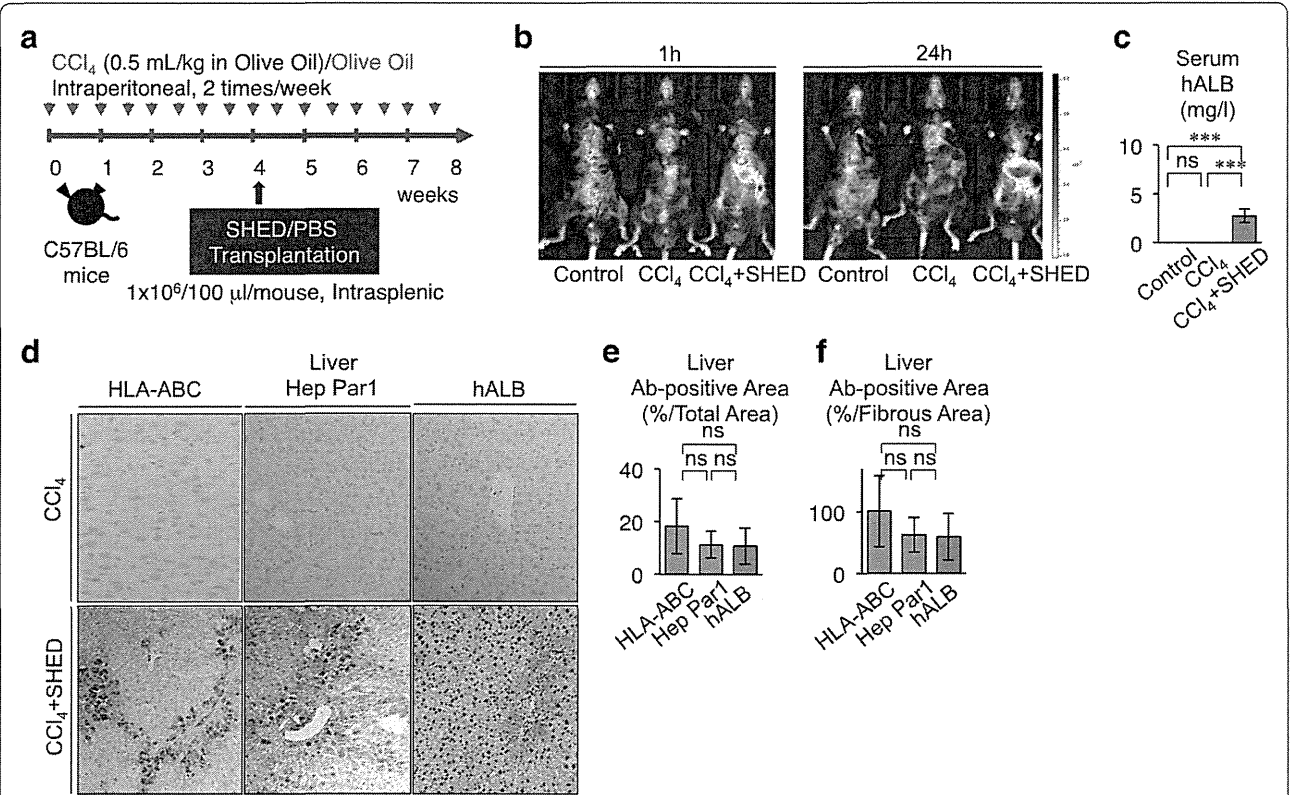


Fig. 1 SHED differentiate into human hepatocyte-like cells in recipient livers of CCl₄-treated mice. **a** Schema of CCl₄ treatment and SHED transplantation in mice. C57BL/6 mice intraperitoneally received CCl₄ (0.5 ml/kg) or olive oil only twice a week (red arrows). Four weeks after the treatment, SHED (1 × 10⁶) were transplanted into the CCl₄-treated mice through the spleen. Phosphate-buffered saline (PBS) was infused as the control for the transplantation. **b** In vivo monitoring of transplanted DiR-labeled SHED in CCl₄-treated mice 1 hour (1h) or 24 hours (24h) after the infusion. Dorsal position. **c** Enzyme-linked immunosorbent assay of human albumin (hALB) in the recipient serum. **d–f** Distribution of transplanted SHED in recipient livers. Immunohistochemistry with anti-human HLA-ABC, anti-hepatocyte paraffin 1 (Hep Par1), or anti-hALB antibody. Representative images. **d** Counterstaining with hematoxylin. The human HLA-ABC, hepatocyte paraffin 1, or hALB antibody positive area. Immunopositive area shown as the ratio to **e** the total area or **f** the fibrous area. **c, e, f** *n* = 5 for all groups. **P* < 0.05 and ****P* < 0.005. *ns* no significance. Graph bars show mean ± SD. Control, olive oil-injected group; CCl₄, CCl₄-treated group; CCl₄ + SHED, SHED-transplanted CCl₄-treated group. *Ab* antibody, CCl₄ carbon tetrachloride, *HLA* human leukocyte antigen, *SHED* stem cells from human exfoliated deciduous teeth

bilirubin were measured with a Multiskan GO microplate spectrophotometer (Thermo Scientific, Waltham, MA, USA) using commercially available kits according to the manufacturer's protocol: ALP, LabAssay ALP Kit (Wako Pure Chemicals); ALT and AST, Transaminase CII-Test Kit (Wako Pure Chemicals); and total bilirubin, Bilirubin QuantiChrom Assay Kit (BioAssay Systems, Hayward, CA, USA). Liver hydroxyproline contents were measured with a Multiskan GO microplate spectrophotometer (Thermo Scientific) using a Hydroxyproline Assay Kit (Biovision, Milpitas, CA, USA). Serum mouse interleukin (IL)-6, IL-10, IL-17, transforming growth factor β 1 (TGF- β 1), and tumor necrosis factor alpha (TNF α) were also measured using Quantikine ELISA kits (R&D Systems, Minneapolis, MN, USA).

Histological and immunohistochemical analyses of mouse liver tissues

Tissue preparation, Masson's trichrome staining, and immunohistochemical staining were performed as described in Additional file 1. The sections were observed under an Axio Imager M2 (Zeiss, Oberkochen, Germany) for morphometric assays, and five representative images from each mouse were selected randomly and were used to measure a percentage of fibrous tissue area or primary antibody-positive area using ImageJ software (NIH, Bethesda, MD, USA). Trichrome stained sections were analyzed to score the amount of liver disease using Ishak scoring [33].

Double immunofluorescence

Double immunofluorescent staining was performed as described in Additional file 1. The sections were observed under an Axio Imager M2 (Zeiss).

Quantitative real-time RT-PCR assay

Total RNAs were extracted and treated as described in Additional file 1. Real-time RT-PCR was subsequently performed using a TaqMan Gene Expression Master Mix (Applied Biosystems, Foster City, CA, USA) and target TaqMan probes (Applied Biosystems) (Table S1 in Additional file 3) with a Light Cycler 96 (Roche, Indianapolis, IN, USA). 18S ribosomal RNA was used for normalization.

Sorting of HLA-ABC-positive or HLA-negative cells from liver tissues of CCl₄-treated mice transplanted with SHED

Livers of primary recipients ($n = 5$) were perfused with collagenase type H (0.1 mg/ml; Worthington Biochemicals, Lakewood, NJ, USA) in PBS and gently dispersed. Single suspended cells were stained with phycoerythrin (PE)-conjugated anti-human leukocyte antigen (HLA)-ABC (eBioscience, San Diego, CA, USA) and magnetic bead-conjugated anti-PE antibodies (Miltenyi Biotec,

Bergisch Gladbach, Germany). They were magnetically sorted using a MidiMACS separator (Miltenyi Biotec) equipped with a LD column (Miltenyi Biotec), and the positive and negative fractions were collected separately.

Cell fusion assay in HLA-positive cells

Magnetically sorted HLA-ABC-positive and HLA-negative fractions were stained with PE-conjugated anti-human major histocompatibility complex (MHC) class I HLA-ABC (eBioscience) and allophycocyanin (APC)-conjugated anti-mouse major MHC class I H-2Kb (eBioscience) antibody. The cells were measured with a FACS Verse flow cytometer (BD Biosciences, San Jose, CA, USA), and were analyzed by BD FACS Suite software (BD Biosciences).

Human-specific genome assay in HLA-positive cells

Genomic DNA was extracted from HLA-ABC-positive and HLA-negative fractions using a DNeasy Blood and Tissue Kit (Qiagen, Venlo, the Netherlands), and was amplified with a T-100 thermal cycler (Bio-Rad, Hercules, CA, USA) using Quick Taq HS DyeMix (TOYOBO, Osaka, Japan) and specific primer pairs by PCR assay. The specific primer pairs are presented in Table S2 in Additional file 3.

Characterization of HLA-positive cells as human hepatocytes

Sorted HLA-ABC-positive cells were cultured with Iscove's modified Dulbecco's medium (Invitrogen, Waltham, MA) supplemented with epidermal growth factor (EGF) (20 ng/ml; PeproTech, Rocky Hill, NJ, USA), fibroblast growth factor 2 (FGF2) (10 ng/ml; PeproTech), and hepatocyte growth factor (HGF) (20 ng/ml; PeproTech). Some cultures were stained with toluidine blue.

Expression of human hepatocyte-specific genes in HLA-positive cells was analyzed by RT-PCR with a T-100 thermal cycler (Bio-Rad) as described previously [16, 23]. The specific primer pairs are presented in Table S2 in Additional file 3. HepG2 cells (Riken, Tsukuba, Japan) were used as positive control. Human albumin and urea in the culture supernatants of HLA-positive cells were measured with a Multiskan GO microplate spectrophotometer (Thermo Scientific) using a Human Albumin ELISA Quantitation Set (AssayPro, St Charles, MO, USA) and a QuantiChrom Urea Assay Kit (Bioassay Systems), respectively.

Secondary transplantation of HLA-ABC-positive or HLA-negative cells sorted from liver tissues of CCl₄-treated mice with primary transplantation of SHED

To understand whether SHED-derived in vivo-converted hepatocyte-like cells express hepatic function in vivo, we performed a secondary transplantation of the SHED-

derived in vivo-converted hepatocyte-like cells into CCl₄-damaged mice. The mice ($n = 5$ each) were treated with CCl₄ for 4 weeks, and were then transplanted with 1 million HLA-positive or HLA-negative cells via the spleen and continuously received CCl₄ twice a week for an additional 4-week treatment after the transplantation (shown in Fig. 6a). We also used CCl₄-treated mice and nontreated mice without the cell transplant ($n = 5$ each). Finally, the peripheral blood serum and liver samples were harvested, and used for further experiments.

In vivo monitoring of transplanted cells

Cells were labeled with near-infrared (NIR) lipophilic carbocyanine membrane dye, 1,1-diiododecyl-3,3,3,3-tetramethylindotricarbocyanine iodide (DiR). The cells (1×10^7 in 10 ml PBS) were incubated with XenoLight DiR NIR Fluorescent Dye (10 μ g/ml; Perkin Elmer, Waltham, MA, USA) for 30 minutes at 37 °C, and were then washed twice with PBS. In vivo optical imaging was performed to detect the transplanted cells. The labeled cells (1×10^6 in 100 μ l PBS) were infused intrasplenically into CCl₄-pretreated mice ($n = 5$). As a control for cell transplantation, nonlabeled SHED (1×10^6 in 100 μ l PBS) were infused into CCl₄-pretreated mice via the spleen ($n = 5$). Ventral images were captured from each animal group after 1 or 24 hours under an optical in vivo imaging system IVIS Lumina III (Perkin Elmer), and were analyzed using living image software (Perkin Elmer).

Statistical analysis

Statistical results are expressed as mean \pm standard deviation (SD). Multiple group comparison was analyzed by one-way repeated-measures analysis of variance followed by the Tukey post hoc test using PRISM 6 software (GraphPad, Software, La Jolla, CA, USA). $P < 0.05$ was considered significant.

Results

Transplanted donor SHED are capable of homing and differentiating into human hepatocyte-like cells in recipient livers of CCl₄-injured mice

Mouse livers showed fibrosis after 4 weeks of treatment with CCl₄ (data not shown). To address a therapeutic potential of SHED for liver disorders, SHED (1×10^6 per mouse) were intrasplenically injected into mice that had been treated with CCl₄ for 4 weeks (Fig. 1a). We first investigated whether transplanted SHED were capable of engrafting in the CCl₄-treated mouse liver parenchyma. DiR-labeled SHED were infused into a spleen of CCl₄-treated mice. In vivo imaging demonstrated that the intensity of DiR was detected on the liver, as well as the spleen, 1 hour after transplantation (Fig. 1b). The signals were enhanced in both the liver and spleen 24 hours

after transplantation (Fig. 1b). Non-CCl₄-treated mice and non-SHED-infused CCl₄-treated mice expressed no signal at 1 and 24 hours after transplantation (Fig. 1b). By the carboxyfluorescein diacetate succinimidyl ester (CFSE)-labeled cell trace technique, CFSE-labeled SHED were detected in CCl₄-damaged mouse liver 1 day after the transplantation (Figure S2 in Additional file 2). Our immunohistochemical analysis also detected positive immunoreactions to anti-HLA-ABC antibody in spleens of CCl₄-damaged mice, but negative immunoreaction to anti-HLA-ABC antibody in spleens of CCl₄-damaged mice (Figure S3B, C in Additional file 2). In addition, no immunoreaction to anti-HLA-ABC and anti-hepatocyte paraffin 1 antibodies was detected in the kidneys and lungs of CCl₄-damaged mice (Figure S3B, C in Additional file 2). These findings suggested that DiR-labeled SHED were recruited to CCl₄-damaged liver from the transplanted site, the spleen.

To confirm in vivo homing of transplanted SHED, peripheral blood serum and liver tissues were harvested from SHED-transplanted CCl₄-treated mice, nontransplanted CCl₄-treated mice, and non-CCl₄-treated mice in week 8. Enzyme-linked immunosorbent assay (ELISA) detected human albumin in the serum of SHED-transplanted CCl₄-treated mice, but not in both nontransplanted CCl₄-treated mice and non-CCl₄-treated mice (Fig. 1c). An immunohistochemical assay demonstrated that HLA-ABC-positive cells with a cuboidal shape were found in the interlobular and portal areas (Fig. 1d), which corresponded to the fibrotic region in CCl₄-injured liver tissues (Fig. 2b). The HLA-ABC-positive cells occupied 16.27 ± 10.17 % of the recipient liver tissues (Fig. 1e). Furthermore, to verify whether the transplanted donor cells differentiated into human hepatocytes in recipient livers, immunohistochemical assay was performed using human hepatocyte-specific hepatocyte paraffin 1 and human albumin-specific antibodies. The hepatocyte paraffin 1-positive and human albumin-positive cells were distributed in interlobular and portal areas of the recipient livers similar to the HLA-ABC-positive cells (Fig. 1d), and were expressed in 11.39 ± 4.58 % and 10.73 ± 6.18 % of the recipient liver tissues, respectively (Fig. 1e). The hepatocyte paraffin 1-positive and human albumin-positive areas tended to be less than the HLA-ABC-positive area, but not significant (Fig. 1e). No immunoreactivity against HLA-ABC, hepatocyte paraffin 1, or human albumin was found in the liver tissue of nontransplanted CCl₄-induced mice (Fig. 1d) or in control mice (data not shown). No immunoreactivity against HLA-ABC, hepatocyte paraffin 1, or human albumin is found for liver sections treated with nonimmune IgG instead of the primary antibodies (Figure S4 in Additional file 2). Positive immunoreaction to anti-HLA-ABC, anti-hepatocyte paraffin 1, and anti-human

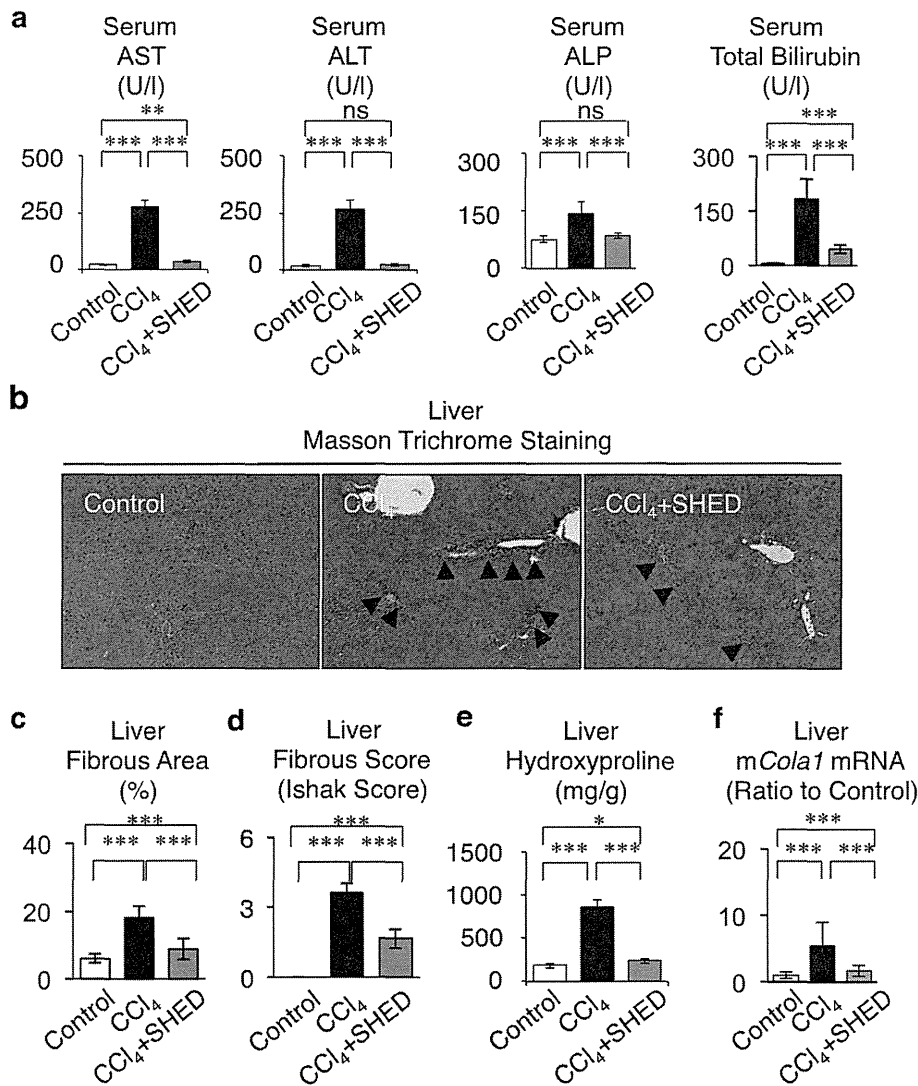


Fig. 2 SHED ameliorate the hepatic dysfunction in recipient livers of CCl₄-treated mice. **a** Serum assays for the hepatic function. **b–f** Liver fibrosis assays. **b** Representative images of livers. Masson Trichrome staining. Arrowheads, fibrous deposition. **c** Fibrotic area. **d** Fibrotic score. **e** Hydroxyproline assay in recipient livers. **f** Real-time RT-PCR analysis of mouse type I collagen (*mCol1*) mRNA in recipient livers. **a, c–f** $n = 5$ for all groups. Control, olive oil-injected group; CCl₄, CCl₄-treated group; CCl₄ + SHED, SHED-transplanted CCl₄-treated group. * $P < 0.05$ and *** $P < 0.005$. *ns* no significance. Graph bars show the mean \pm SD. ALT alanine aminotransferase, ALP alkaline phosphatase, AST aspartate aminotransferase, CCl₄ carbon tetrachloride, SHED stem cells from human exfoliated deciduous teeth

albumin antibodies was detected in almost of parenchymal cells of human liver tissues (Figure S5 in Additional file 2), but human liver tissues expressed negative immunoreaction to nonimmune mouse IgG (Figure S5 in Additional file 2). These results indicated that donor SHED showed an in vivo capacity of engrafting and differentiating into human hepatocyte-like cells in the recipient livers of CCl₄-injured mice.

SHED transplantation decreased CCl₄-induced chronic fibrosis in mouse livers

To address whether SHED have therapeutic potential for liver disorders, SHED-transplanted CCl₄-treated

mice, as well as nontransplanted (PBS-injected) CCl₄-treated mice, received continuous CCl₄ injections for an additional 4 weeks (Fig. 1a). In week 8, the nontransplanted mice showed severe fibrous liver dysfunction (Fig. 2). A biochemical serum assay revealed that SHED transplantation markedly recovered the damaged liver functions (Fig. 2a). Masson trichrome staining showed that SHED transplantation reduced CCl₄-enhanced fibrous deposition in the liver (Fig. 2b, c). The fibrous tissue area occupied 5.98 ± 1.35 %, 18.16 ± 3.36 %, and 8.89 ± 3.07 % of the recipient liver tissues in control mice, nontransplanted CCl₄-treated mice, and SHED-transplanted CCl₄-treated mice, respectively (Fig. 2c).